Nederlandse Organisatie voor
toegepast-natuurwetenschappelijk
onderzoek / Netherlands Organisation
for Applied Scientific Research

TNO Defence, Security and Safety

Lange Kleiweg 137
P.O. Box 45
2280 AA Rijswijk
The Netherlands

www.tno.nl

T +31 15 28 43000
F +31 15 28 43991
Info-DenV@tno.nl

TNO report

DV2 2005-A13

Analysing blast and fragment penetration effects on composite helicopter structures

Date	March 2005
Author(s)	C. van 't Hof, K. Herlaar, J.M. Luyten, M.J. van der Jagt
Classification report	Ongerubriceerd
Classified by	Lkol J.C.E. Helderman
Classification date	17 February 2005 (This classification will not change)
Title	Ongerubriceerd
Managementuittreksel	Ongerubriceerd
Abstract	Ongerubriceerd
Report text	Ongerubriceerd
Appendices	Ongerubriceerd
Copy no	6
No. of copies	21
Number of pages	70 (incl. appendices, excl. RDP & distributionlist)
Number of appendices	4

DISTRIBUTION STATEMENT A
Approved for Public Release
Distribution Unlimited

The classification designation Ongerubriceerd is equivalent to Unclassified

MANAGEMENTUITTREKSEL

Het analyseren van scherfinslag en explosiedrukuitwerking op composiet helikopterconstructies

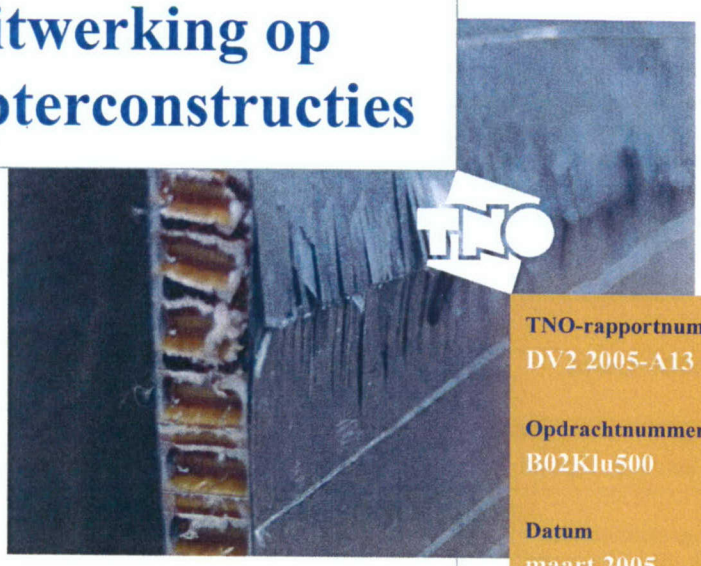

TNO-rapportnummer
DV2 2005-A13

Opdrachtnummer
B02Klu500

Datum
maart 2005

Auteur(s)
ir. ing. C. van 't Hof
ir. K. Herlaar
ir. J.M. Luyten
ir. M.J. van der Jagt

Rubricering rapport
Ongerubriceerd

Probleemstelling

In het hedendaagse gevechtsveld is de helikopter uitgegroeid van observatiemiddel naar multifunctioneel platform. Met het toegenomen belang van helikopteroperaties vinden belangrijke verschuivingen plaats op het gebied van zowel dreiging als kwetsbaarheid:

1. De dreiging komt steeds dichter bij de helikopter. Waar het risico voorheen was beperkt tot schade door scherfinslag, speelt nu ook explosiedruk (blast) een rol van betekenis.
2. Bij de constructie van helikopters worden steeds meer metalen delen vervangen door composietmateriaal. Dit heeft niet alleen gevolgen voor de manier van construeren, maar ook voor de kwetsbaarheid.

Deze ontwikkelingen vereisen aanpassing van de kwetsbaarheidsmodellen. Doel van voorliggende studie is om de gevolgen van zowel blast als scherfinslag op een composiet paneel te bepalen. Gebruik wordt gemaakt van Eindige Elementen Methoden (EEM's) en kleinschalige experimenten. De te ontwikkelen methoden dienen aanvullend op en samenwerkend met de huidige kwetsbaarheidmodellen te zijn.

Beschrijving van de werkzaamheden

De werkzaamheden bestonden uit een combinatie van numerieke berekeningen en experimenten die de interactie tussen de dreiging (blast, scherven) en doel (composiet paneel) simuleren. Bovendien is een aantal kleinschalige testen uitgevoerd om materiaalparameters te bepalen, noodzakelijk als input voor de simulaties.

Blastuitwerking

Het uitgangscomposiet voor dit onderzoek is gebaseerd op de sandwichconstructie die wordt toegepast in het dragende deel van de Cougar-helikopter. Een numerieke EEM (LS-Dyna) is gebruikt om de blastuitwerking op het sandwichpaneel te simuleren. De resultaten geven de uitbuiging, de plaats en het moment van falen weer. Experimenteel is de respons van het sandwichpaneel bepaald in de blastsimulator van TNO Defensie en Veiligheid, locatie Rijswijk. De experimentele en numerieke resultaten zijn onderling vergeleken.

Scherfinslag

Bij het onderzoek naar de impact van een scherf op een composiet paneel is gebruik gemaakt van een reeds getest paneel Error! Reference source not found., kenmerkend voor een helikopterconstructie. De impact van een Fragment Simulating Projectile (FSP) op het composiet paneel is gesimuleerd, gebruikmakend van het EEM AUTODYN waarbij de inslag- en restsnelheden van het projectiel en het schadegebied van het composiet paneel zijn bepaald. Voor de simulatie zijn de noodzakelijke materiaalparameters bepaald aan de hand van kleinschalige testen en literatuurstudies.

Resultaten en conclusies

Blastuitwerking

De experimentele resultaten tonen een goede overeenkomst met de numerieke resultaten en bieden veel inzicht in het faalgedrag van sandwichpanelen onder een explosiebelasting. Uit de studie volgen de uitbuiging en het moment van bezwijken. Ook laat de studie zien dat het bezwijken ontstaat door het knikken van de op druk belaste vezels.

Scherfinslag

De berekende en experimentele resultaten zijn onderling vergeleken en zijn consistent voor de uittree-snelheden van het projectiel. De

grootte van het schadegebied heeft zowel experimenteel als numeriek dezelfde omvang. Echter, bij een toenemende impactsnelheid geven de numerieke en experimentele resultaten verschillende trends aan. Analyse van dit probleem geeft aan dat een aantal extra materiaalparameters experimenteel moet worden bepaald, omdat ze grote invloed hebben op de grootte van het schadegebied.

Kennis is opgebouwd met het simuleren van de response van scherfinslag en explosiebelasting op composiet helikopterpanelen. De studie maakt het mogelijk om in de toekomst de kwetsbaarheid van composiet helikopterconstructies te simuleren waardoor een aantal kostbare experimenten kan worden verminderd.

Toepasbaarheid

PROGRAMMA	PROJECT
Programmabegeleider Lt-kol. B.H. Hoitink, KLu	Projectbegeleider Lt-kol. Ing. J. Helderman, KLu
Programmaleider R. le Fevre, TNO Defensie en Veiligheid, lokatie Den Haag	Projectleider ir. J.M. Luyten, TNO Defensie en Veiligheid, lokatie Rijswijk, Business Unit Wapens, Munitie en Bescherming
Programmatitel Helikopters: tactieken, planning en logistiek	Projecttitel Gedrag van Composietmaterialen
Programmanummer V015	Projectnummer 014.14186
Programmaplanning Start 01-01-2001 Gereed 01-03-2005	Projectplanning Start 01-06-2004 Gereed 01-03-2005
Frequentie van overleg Met de projectbegeleider werd 1 maal gesproken over de invulling en de voortgang van het onderzoek.	Projectteam ir. K Herlaar, ir .ing. C. van 't Hof, ir. M.J. van der Jagt. Meetteam: J.N.A. van Leeuwen, E.C.M. van Daelen, TNO Defensie en Veiligheid lokatie Rijswijk, Business Unit Wapens, Munitie en Bescherming

TNO

Lange Kleiweg 137
2288 GJ Rijswijk
Postbus 45
2280 AA Rijswijk

www.tno.nl
www.pml.tno.nl

T 015 284 28 42
F 015 284 39 91
E info@pml.tno.nl

Contents

1 Introduction

1.1 General introduction

Sandwich structures become increasingly important as structural parts in helicopters. This does not only have effect on the way of construction but also on the vulnerability of the helicopter. The last decades the threat on helicopters has increased in military circumstances. Consequently the helicopters will be exposed to weapon effects like high blast loads and fragment impact more frequently. Moreover the blast load becomes more important because the threat comes closer to the target.

At TNO different blast and fragment response models are available for metal structures. However little is known about the blast performance of sandwich panels. To be able to determine the damage of these structures due to blast loads and fragment impact it will be necessary to extend the present vulnerability methods for composite structures.

Within the Helicopter programme V015 a project was set up to study the behaviour of composite helicopter structure [1]. The objective of this project is to develop and evaluate methods, which can simulate response of composite helicopter structures caused by projectile impact and blast. The project is split into a blast and a fragment impact study, introduced in Section 1.2 and Section 1.3, respectively.

1.2 Blast load on sandwich panels

Firstly, the present study aims at gaining insight in the behaviour of sandwich panels under blast loading. Secondly, it is a first exploration into modelling composites and composite failure in a finite element code (LS-Dyna). Comparison of experimental results with numerical results should increase our understanding of the processes appearing in both.

Helicopter sandwiches often consist of a Nomex honeycomb core in between two (carbon) fibre reinforced polymer facings. The advantage of sandwiches is an increased bending stiffness of the structure, relative to that of the facings alone, without a large mass penalty.

In current military helicopters relatively small sandwich panels are mounted on a, whether or not composite, frame. For this purpose, the panels are tapered at the edges, i.e. at the end of the honeycomb core one of the facings is bended towards the other to obtain a trough-thickness stiff mounting surface. The cavity in this tapered sandwich end is usually filled with some thermosetting resin.

In future helicopters large parts of the fuselage are expected to be made from sandwich structures, without a supporting frame. In other words, the panel edge becomes probably less important. For this reason, the present study focused on the global behaviour of the sandwich panel, rather than on the behaviour of its supported edge.

In the present work particularly the bending behaviour of sandwiches under blast loads was studied. The panels were one-way, simply supported along their longest sides. Bending is thus over its shortest span for maximum probability of failure before the

panel leaves the supports: given some fixed value for l_p-l_s, where l_p the panel length and l_s the distance between the supports, the panel curvature at the time the panel leaves these supports will be larger for smaller l_s.

The approach was the following. Initially some preliminary FEM simulations were performed to be able to order sandwich panels suitable for testing on the blast simulator. These simulations are not reported in the present report, but are rather similar to those performed later on. The sandwich details are described in Chapter 1.

Secondly, the ordered panels were tested on the so-called blast simulator. Tests and results are described in section 3and 4, respectively.

At last, numerical simulations were performed, using blast loading curves as measured during the experiments. Modelling details and simulation results are described in sections 5 and 6, respectively. Section 7 summarizes the comparison between experimental and numerical studies.

This memorandum is closed with some conclusions and recommendations for future studies.

1.3 Fragment impact on composite material

The damage caused by projectile impact will be modelled with a material model for fibre reinforced materials named ADAMMO in the simulation code AUTODYN. This work is reported in Section 8 and 9.
Before simulations can be done a number of input data is needed. First a choice of composite material should be made. For this material the input data for the material model is needed, like engineering constants, failure criteria and Equation of State (EOS). If these material parameters are not known than they have to be determined with material tests if possible.
Second ballistic test results are needed to verify the outcome of the model. To verify the internal damage predicted by the model non-destructive inspection with a C-scan (ultrasound) of one or more panels should be performed. Because of budgetary and time limitations only one panel is inspected with the C-scan.

2 The sandwich panels

Two honeycomb sandwich panels were ordered at Holland Composites International, Lelystad. As mentioned before, these sandwiches consist of a Nomex honeycomb core in between two carbon fibre reinforced polymer facings. The honeycomb used is representative of that used in the so-called 'intermediate structure' of the Cougar helicopter. This intermediate structure is the connection between the fuselage and the tail boom.

The sandwich panels will be simply supported along their longest sides during the blast experiments. To be able to withstand the enormous transverse forces transferred by the supports, the relatively weak honeycomb was replaced by wooden inserts along the supported edges. All relevant panel details are shown in the picture in Appendix A and in Table 1 below.

Table 1 Details of sandwich panels constituents.

Dimensions	1145 x 904 x 13 [mm]
Facings	UD Carbon – Epoxy
Stacking sequence	90°/45°/-45°/0°/Honeycomb/0°/-45°/45°/90° (see Appendix A)
Carbon	UD Carbon T 700, 150 [gr m^{-2}], Heinsco LTD, UK
Resin	Rütapox 0164/S 700, hardener 14% Rütadur DPTA, Bakelite AG
Honeycomb	Nomex HRH-10-3/16-12, ANC
Wooden inserts	Merbau or Mirabow wood
Glue	Rutapox 0164/S 700, Bakelite AG, hardener 40% Euredur 14, Ciba, Aerosil (ca 5%)

Honeycomb is an orthotropic material. Its principal directions are the 'tubular' or T-direction, the L-direction, which coincides with the direction in which the honeycomb cell walls are glued together, and the W-direction, perpendicular to L. See also Figure 1. The orientation of the honeycomb in the sandwich structure is such that the stiffer L-direction coincides with the 90°-direction of the panel, see also Appendix A.

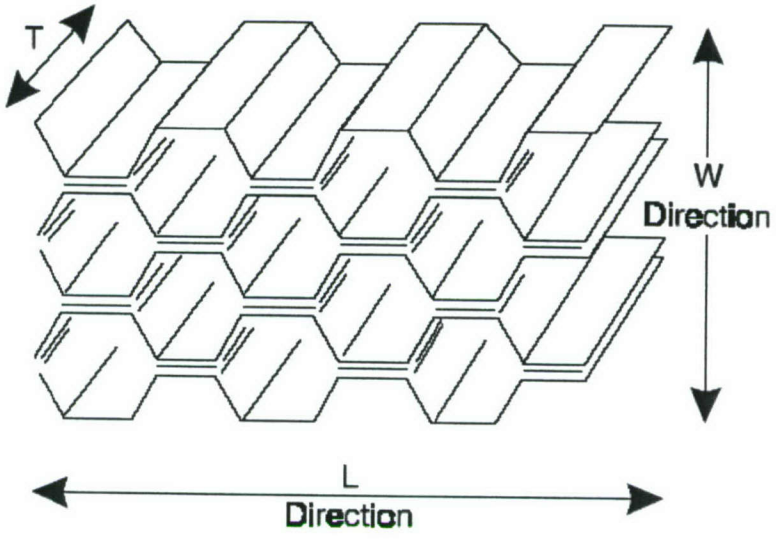

Figure 1 Honeycomb principal material directions, picture copied from www.hexcelcomposites.com

The facings were made by vacuum injection on an aluminium table. Curing took place at room temperature. Subsequently the facings, honeycomb and wooden inserts were glued together, also at room temperature and at 60% vacuum pressure. The Aerosil was added to the glue to obtain a workable viscosity. After curing of the glue the panel was sawed to the right dimensions.

3 Blast Experiments

The sandwich panels were subjected to blast loads, with a twofold objective. The first is, of course, to gain insight in the (failure) behaviour of this kind of panels under blast loads. The second is to verify the FE simulations performed, by comparing characteristic features in simulations and experiments, e.g. deflections and failure locations. To be able to measure the chronological deflection pattern and to detect time and location of failure, camera recordings of the panel, equipped with retro reflective stickers, were made. Blast loads applied were measured to be used as input in the FE simulations.

Blast loads can be generated by the so-called blast simulator. This blast simulator, see Figure 2, is operated by TNO location Rijswijk, and was originally designed for producing blast waves with a relatively long positive phase, in the order of 70 – 90 [ms]. The wave is generated by detonating an acetylene-oxygen mixture in the combustion chamber. The blast simulator has a high reliability and reproducibility and can be operated at low costs, which are important advantages over for instance high-explosive experiments in a closed bunker.
The blast wave travels through a 63 [m] long pipe that widens in a stepwise manner to a final 2 [m] diameter. Against the end face of the pipe a so-called 'mask' is placed, a thick steel plate with a central opening. There are several masks, each with a different opening size. The mask selected for the current test has a rectangular 1000 × 800 [mm] opening.

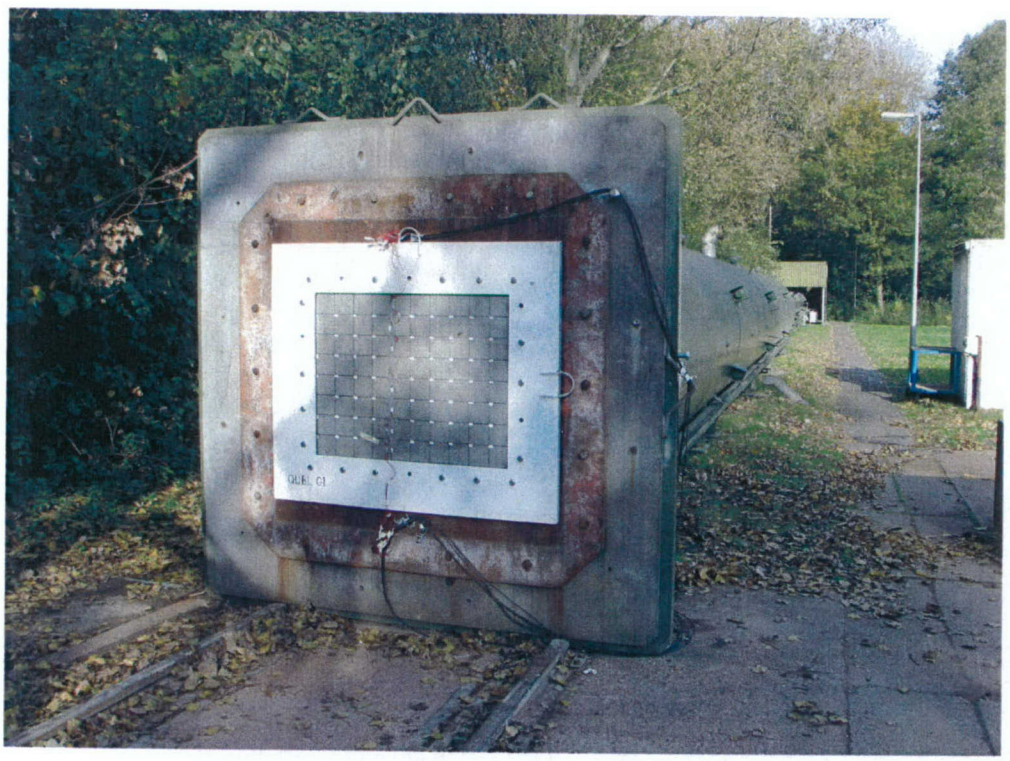

Figure 2 The blast simulator (not with the sandwich panel used in the present work).

The sandwich panel was pressed against two horizontal 'simple supports', mounted on the mask as shown in Figure 3 and Figure 4, by means of stacked wood (as spacer) and rubber strips between the vertical panel edges and the mask. The light-coloured wooden strip is clearly visible in Figure 4.

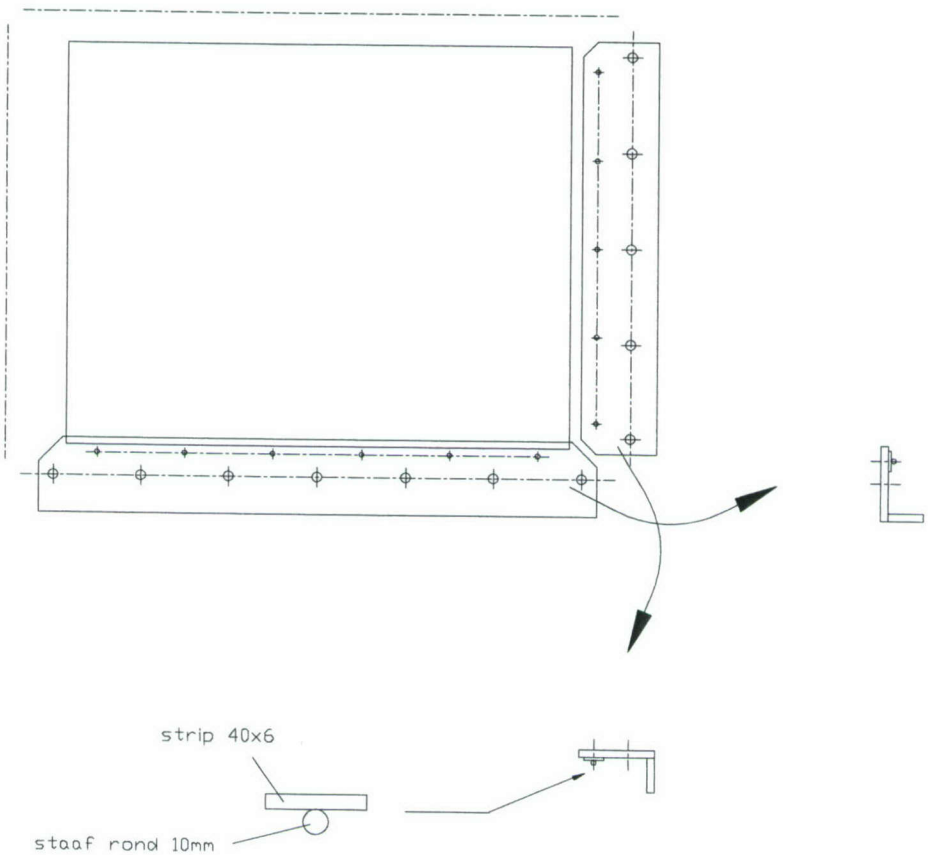

Figure 3 Simple support of panel on the blast simulator's mask.

Figure 4 Experimental set-up. The panel is pressed against its supports using wood (light coloured) and rubber strips at the vertical edges. In the front the camera can be seen. The halogen light spots are mounted on the camera frame.

A safety net, as used in the construction industry, was hanged in front of the opening in the mask to catch the panel after being released from its supports. See also Figure 4. This was done in order to prevent the panel from being damaged by other means than the blast load.

Two pressure transducers (Endevco, type 8530C) were used to measure the reflected pressure on the mask and the side on pressure.

During the tests high speed camera (Redlake MotionXtra HG-LE) colour recordings were made at 3000 frames per second. The camera was positioned such that its optical axis made an angle of 36° with a normal on the test panel, in the horizontal plane. See also Figure 4.

From the recordings, both the chronological ordering of the response as well as a more or less quantitative deflection pattern were obtained. For the latter, the panel was equipped with so-called 'retro reflective stickers', which give clear reflections in the direction of a light source. In this case two 250 [W] halogen light spots were placed close to the camera. By tracking the position of the stickers in the pictures and the use of some goniometry, the deflection of the panel can be derived. Tracking was performed by selecting pixels with specific properties (light intensity or transitions), by means of the software package MiDAS, from XCITEX. The whole panel was lighted by a 2.5 [kW] HMI floodlight from ARRI.

Verification of the FE simulations falls apart in two subparts. On the one hand the verification of the sandwich model, including the shell formulation, lamina stacking sequence, some lamina properties and the boundary conditions. On the other hand the verification of the implemented composite failure model, with an additional set of lamina properties. For verification of the LS-Dyna sandwich model a reversible, i.e. elastic response is necessary.

Preliminary numerical studies showed that at a reflected pressure of 30 [kPa] failure was already expected. The first experiment therefore aimed at the lowest pressure possible: 22 [kPa] was obtained. The first out of the two panels survived the test without any visible damage and could thus be used in a second test.

To investigate the effects of a 'real' blast load, the same panel was loaded with the maximum pressure in a second experiment. This test led to severe damage.

Since the preliminary numerical studies showed failure at 30 [kPa], the second panel was loaded slightly higher to check if failure would appear indeed. The results of this experiment could act as a reference in the verification of the composite failure model. A pressure of 37 [kPa] was obtained in this experiment.

Table 2 Measurement program for blast tests.

Measurement	Panel	Pressure peak	Aims at:
1	1	22	Elastic response
2	1	121	Visualizing 'real' blast damage
3	2	37	Failure initiation

4 Experimental Results

Panel 1 test 1

During this test the panel did not release from its supports. From the camera recordings the maximum deflection of 89 [mm] appeared after 7.7 [ms]. The panel jumped to and fro a number of times. Optically, no damage could be observed. Albeit somewhat subjective, knocking on the panel indicated the latter still was a firmly laminated structure. It was decided to use the panel for another test: Panel 1, test 2.

The blast pressure signal as recorded during the experiment is shown in Figure 5.

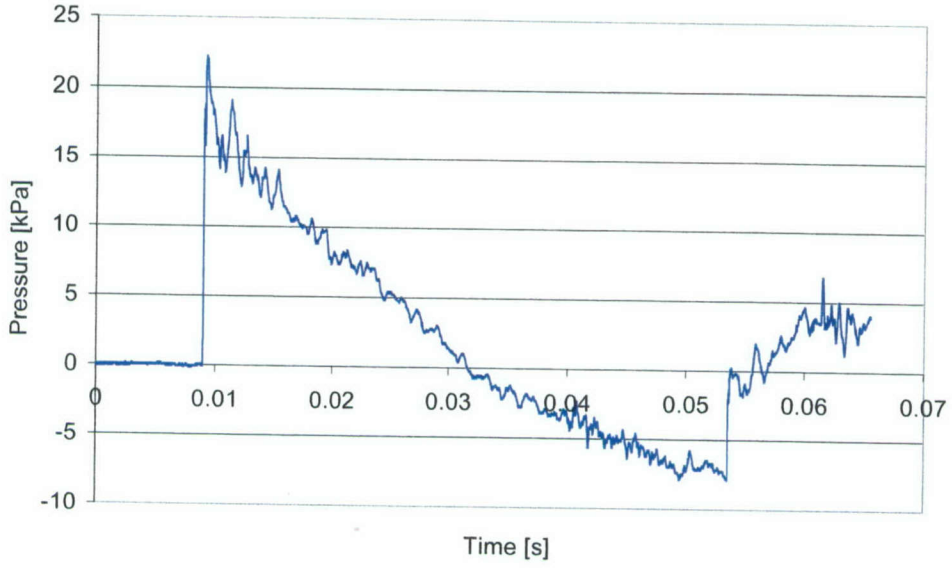

Figure 5 Reflected pressure recordings of experiment 1, i.e. panel 1 test 1.

Panel 1 test 2

During this test the panel bent globally, folded and released from its supports, see also the sequence in Figure 6. It was caught by the net which is, in turn, partly cut by the panel or by the panel edges.

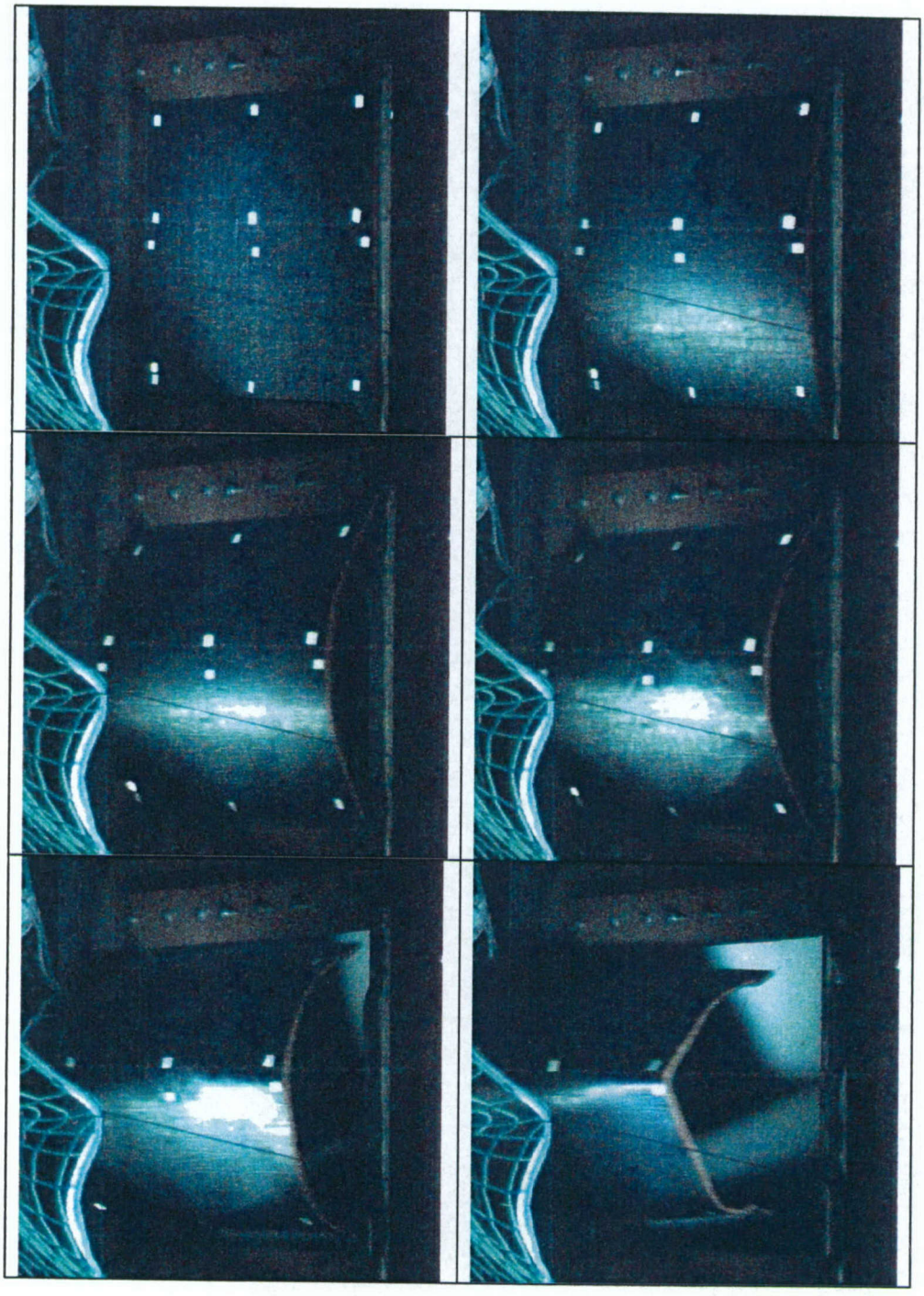

Figure 6.a-f Deflection sequence of panel 1, test 2. Times are 0, 2.3, 3.7, 4.0, 5.3 and 7.7 [ms].

From the camera recordings the exact location of failure initiation is hardly visible. It is expected to appear close to the point of intersection of the panel edge and the black wire used to tighten the net, in Figure 6c. Failure initiates probably after 3.3 [ms], the deflection at $t = 3.3$ is 143 [mm]. It can be observed that secondary folds appear in the

panel approximately 100 [mm], i.e. 1/8 of panel height, from the supported edges, either due to regular blast loads on the supported panel or due to collision of the panel with the mounting frame of the supports.

Some remains of paint on the panel indicate clearly that the panel has come into contact with the mounting frame of the supports. Moreover, small remains of green fibres from the net indicate firm contact between the net and the panel.

Damage Observations

After this test, the panel is severely damaged, see also Figure 7. However, the panel's 'outer' side, i.e. facing open air, is almost completely intact, except at some locations at the edge and except a severe local indentation, where the panel probably hit the chain used to tighten the net, see also Figure C.1 in Appendix C.

At the inner, blast loaded side, shown in Figure 7, there are two large folds on the left hand side, converging to one on the right hand side. On that right hand side, fibre buckling seems to have appeared. In the lower left fold, fibre tear off seems to have occurred. In the upper left fold it is not clear what actually happened, the facing seems to have just folded, perhaps with some very small buckling effects.

It is remarkable that the secondary folds, clearly visible in Figure 6f, did not cause any visible damage in the facings.

In large areas the honeycomb is crushed, as can be seen along the panel edge and heard by pressing on other parts of the panel. The wooden inserts are partly delaminated, whereas the facings at that location are still intact. See also Figure C.1 to Figure C.8 in Appendix C.

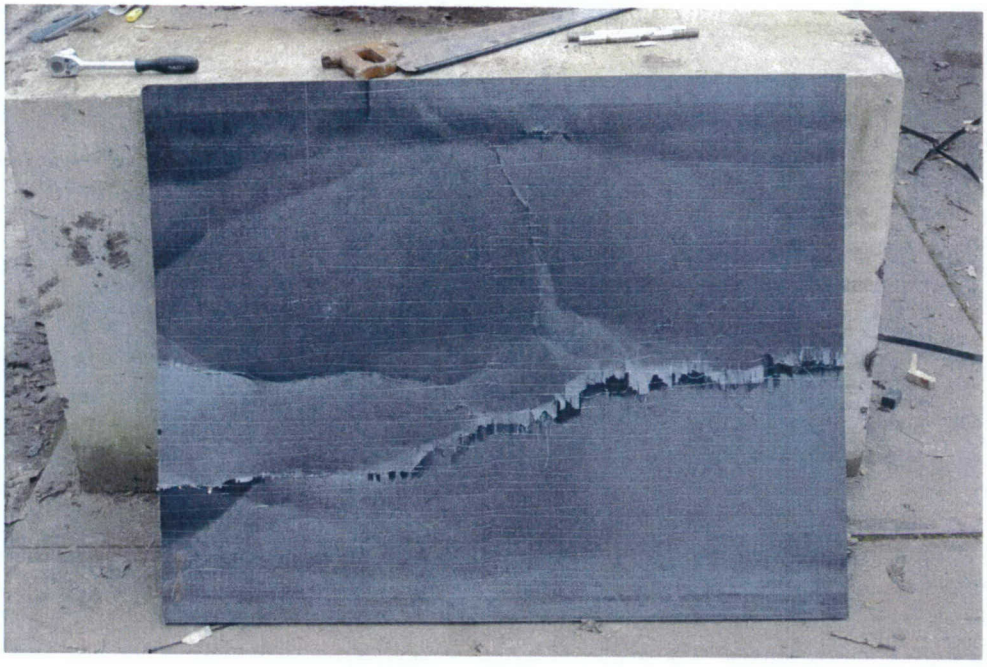

Figure 7 Panel 1 after test 2, blast loaded side.

As can be seen from Figure 7, folds have more or less arbitrary orientations, in the sense that they are not directed by the horizontal 'hold together' wires[1] or the 45° lamina, effects that are clearly observed in the next test.

Generally, the damage pattern observed obeys the expectations according to static engineering mechanics, i.e. bending failure along the horizontal centre line or shear failure in the core close to the horizontal edges, to a much lesser extent than will be observed in the next test. The dynamics of the blast process could be the reason for the global state of damage as observed, although part of the damage may also be attributed to contact with the safety net or the collision with the supports' frames. The latter two possibilities significantly complicate the interpretation of the observed damage in this experiment.

The blast pressure signal as recorded during the experiment is shown in Figure 8.

---

1 These wires hold together the otherwise unconnected UD carbon fibres. They are clearly visible in Figure 12.

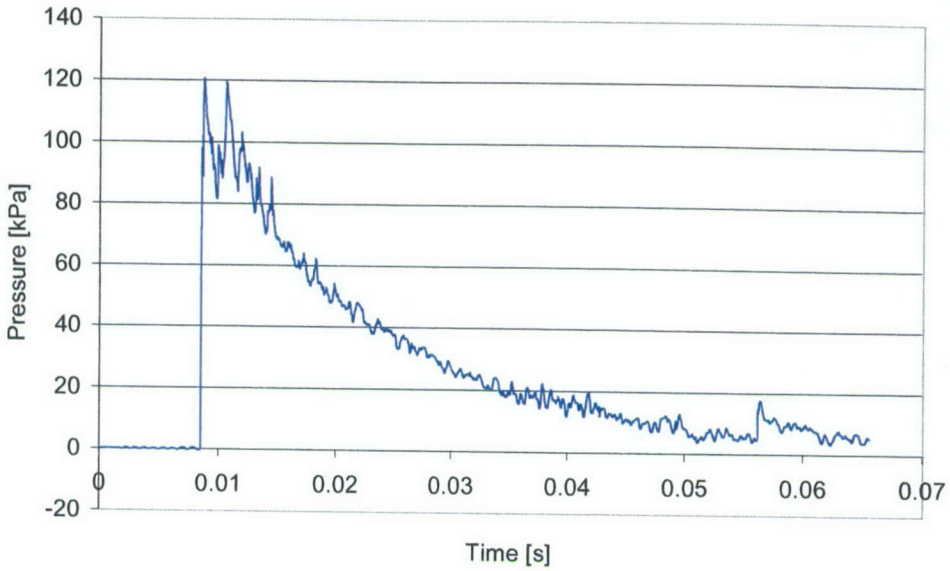

Figure 8 Reflected pressure recordings of experiment 2, i.e. panel 1 test 2.

Panel 2 test 1

In this test the panel initially bent globally, then folded and subsequently released from its supports, see also the sequence in Figure 10. Afterwards, the panel was nicely caught by the safety net, as can be seen in Figure 9.

Figure 9 Panel 2 is nicely caught by the safety net.

From the camera recordings the maximum deflection before failure, i.e. 135 [mm], occurred after 6.3 [ms]. As can be seen in the frame sequence below, the start of failure is clearly visible. The curvature of the entire plate, in Figure 10c, concentrates around a horizontal line in Figure 10d; the panel is folded. Afterwards the upper and lower halves of the plate become more or less flat again (Figure 10d - Figure 10f).

From the recordings, it is hard to say at what time the panel released from its supports. Again, some remains of paint on the panel clearly indicate that the panel has come into contact with the mounting frame of the supports.

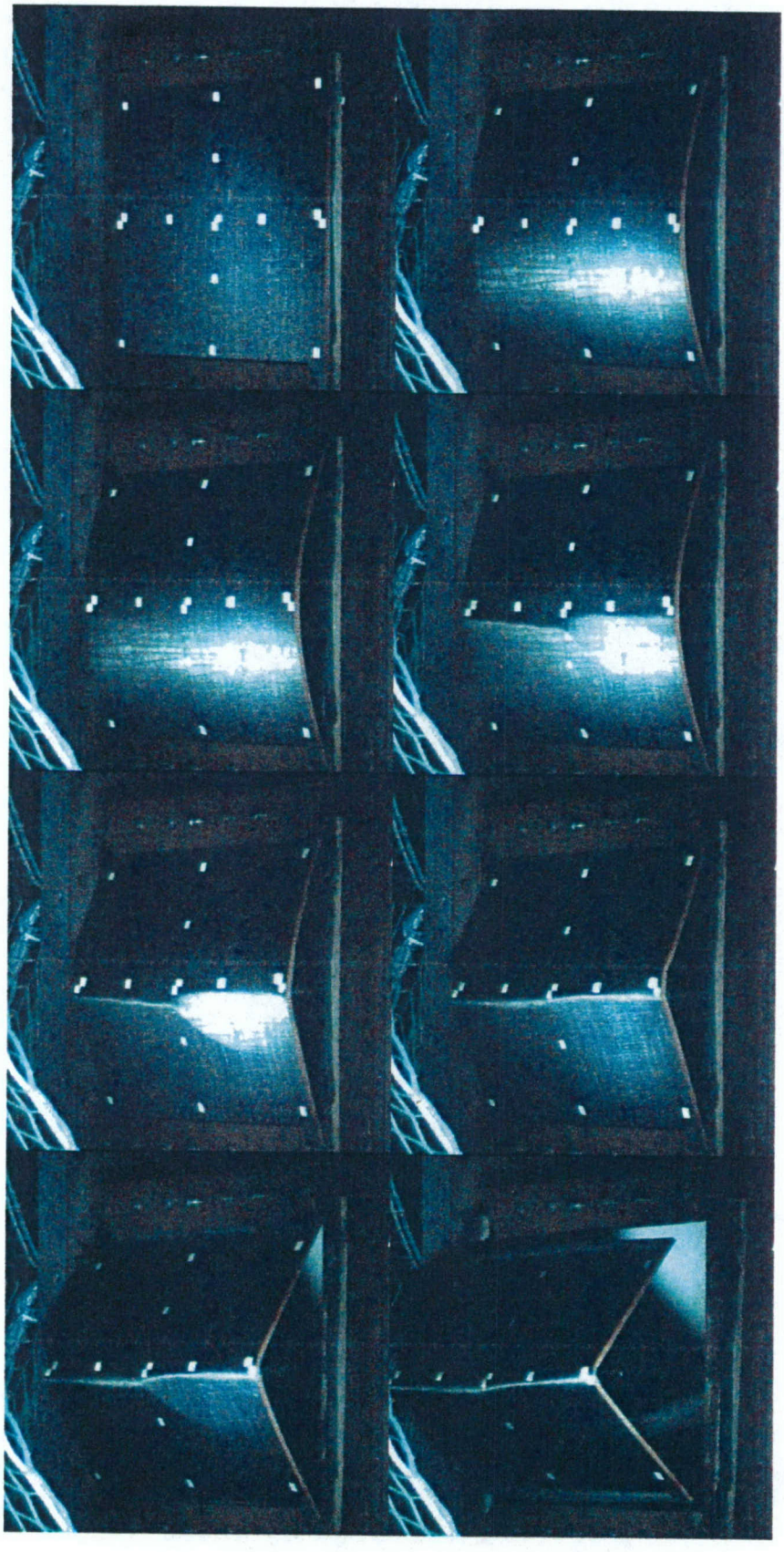

Figure 10.a-h High speed camera sequence of panel 2, test 1. Recording time of frames: 0, 6.0, 6.3, 7.0, 7.7, 8.7, 12.3 and 19.0 [ms].

Damage observations

Surprisingly, no damage is visible in the tension loaded facing. Apparently this facing can survive the rather small bending radius as observed during 'flight' even without visible delamination.

The compression loaded facing has failed primarily along the horizontal centre line, see Figure 11. This failure allowed the panel to fold during the test.

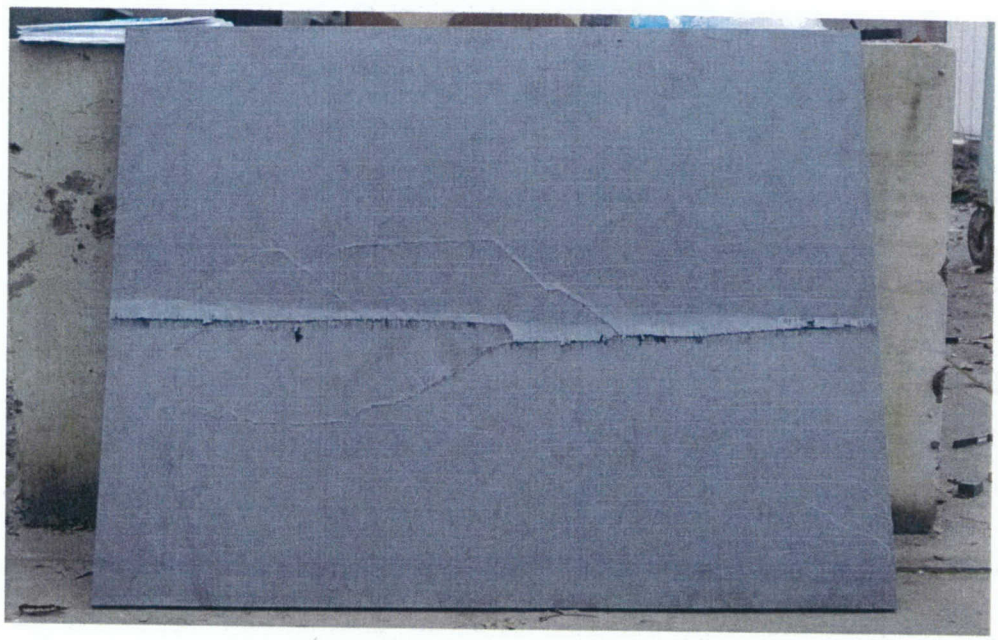

Figure 11 Panel 2 after testing, blast loaded side.

The failure mechanism seems to be fibre buckling, see also Figure 12, at least for the outer (90°) layer. Buckling is initiated at the 'hold together' wires, and at the same location the lamina are (finally?) broken. At the buckled locations, delamination between the facing layers seems to have appeared.

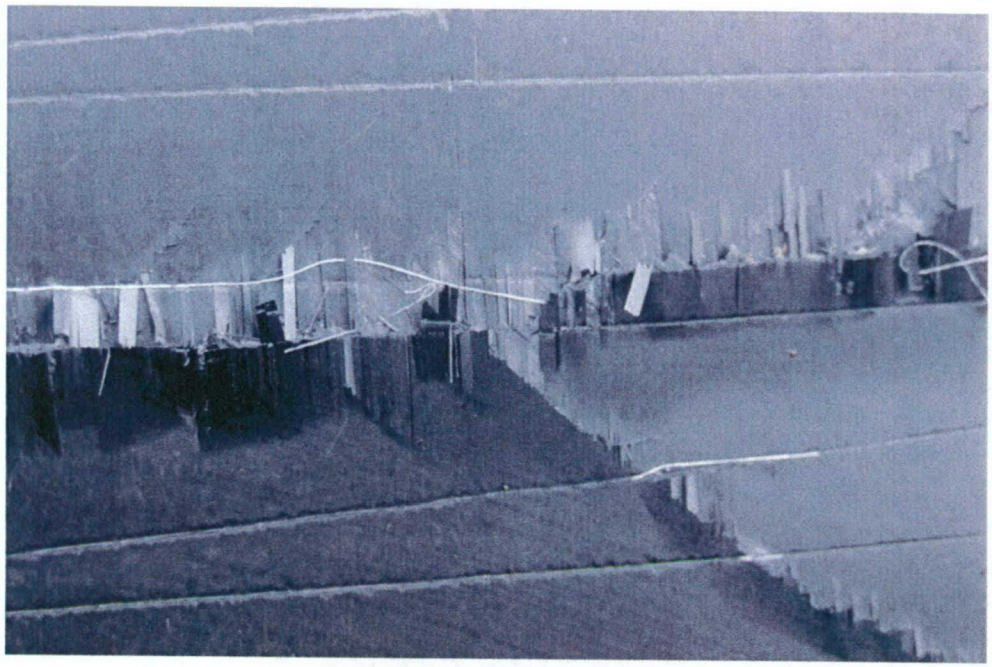

Figure 12 Close up of failure at blast loaded panel side.

In this test, some minor buckling lines emerge from the horizontal centre 'fold'. These lines clearly follow the directions from either the 'hold together' wires or the 45° layer. In the latter case, failure of the 45° layer probably preceded the buckling of the 90° layer.

At the ends of the main 'fold', the damage of the honeycomb is visible. Delamination between facing and honeycomb seems to have occurred, but at one side also in-plane 'cracks' are observed in the honeycomb. To be able to fold during flight, the honeycomb has to be locally crushed. This clearly happened; the honeycomb lost its stiffness almost completely.

Figure 13 Honeycomb damage at the end of the main fold. In-plane cracks and local delamination and crushing are observed.

The blast pressure signal as recorded during the experiment is shown in Figure 14.

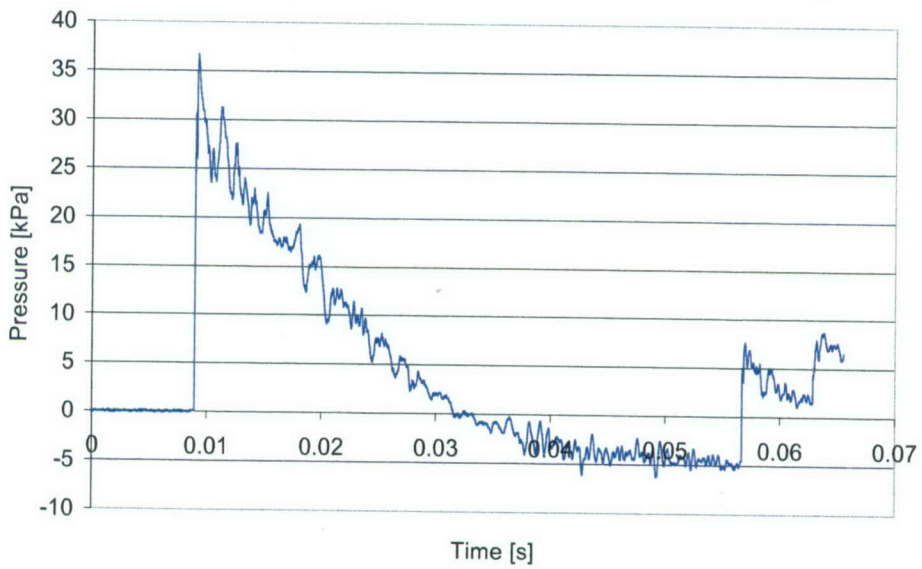

Figure 14 Reflected pressure recordings of experiment 3, i.e. panel 2 test 1.

5 Finite Element Modelling

Given an accurate material model, the finite element method is a powerful tool to study the behaviour of structures of arbitrary geometry under more or less arbitrary loading conditions, studies usually too expensive to perform experimentally. By means of a number of well-chosen, simple experiments, one needs to get confidence in the modelling approach used. In the present work, the performance of LS-Dyna in modelling the blast behaviour of sandwich panels is compared to the experiments as described in Chapters 2 and 3.

A quarter of the sandwich panel was modelled using LS-Dyna, version 970, by 10×10×13 [mm] shell elements. Element type 16, i.e. a fully integrated shell element, was used. The 13 [mm] thickness is build up by 8 lamina, each 0.125 [mm] thick, and the 12 [mm] thick honeycomb core.

As material model, material 54-55, i.e. *mat_enhanced_composite_damage, is used. In this material model both the stacking/orientation of the different layers as well as their mechanical and failure properties are specified. Each layer is attributed to (at least) one integration point of the shell formulation.

Estimates for the properties of the UD Carbon – Epoxy lamina are obtained from CompositePro, a software tool for preliminary composite design. They are summarized in Table 14, see Appendix B. Most of the material properties for the honeycomb are obtained from www.HexcelComposites.com, indicated in Table by 'HC'. Some, less important, values were assumed, as indicated by an 'A' in the same table. For the properties for the wooden (Merbau or Mirabow) inserts, those of red oak are used, because of lacking data for Merbau. See Table, also in Appendix B. Wood properties are characterized by large scatter, anyway.

The support is modelled by the contact algorithm *contact_nodes_to_surface, between the shells and a set of simply supported rod elements, see also Figure 15.

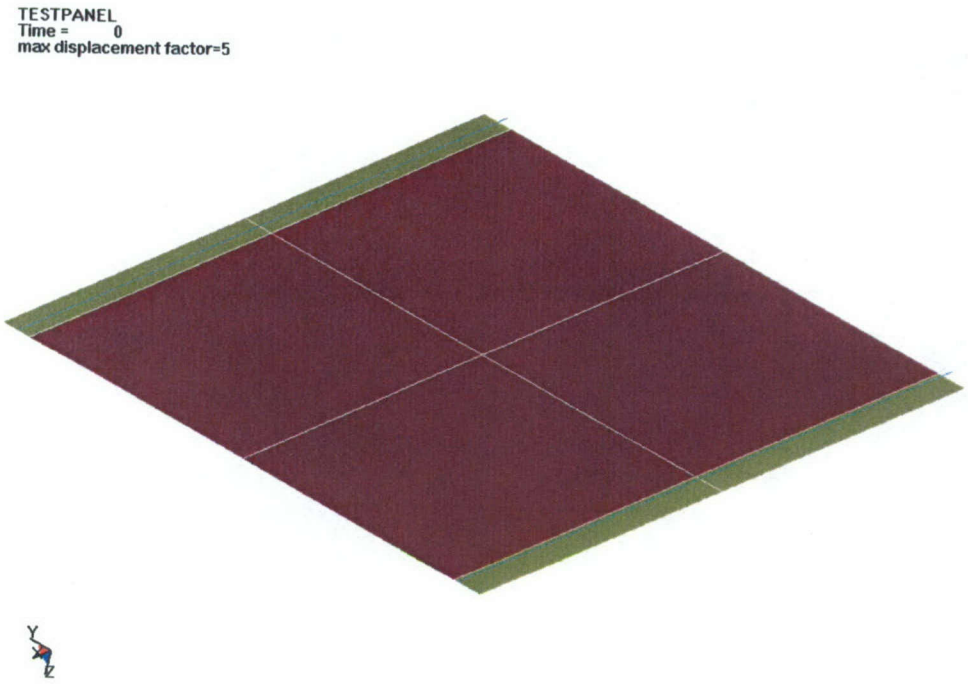

Figure 15 Geometry of the FE model. Red surface: sandwich with honeycomb core, green surface: sandwich with wooden insert, blue line: supports with rod elements.

The blast pressure is assumed to be homogeneously distributed over the sandwich' surface. For the preliminary simulations, mentioned in Chapter 3, a scaled pressure versus time curve from former experiments was used [13]. For the simulation of the experiments performed in the present work, approximations of the experimentally obtained curves, see Figure 5, Figure 8 and Figure 14 were used.

Verification of FE sandwich model with analytical approximation

To have some confidence in the correct implementation of all material and geometrical input, a quasi-static FE calculation was compared to an analytical approximation as can be obtained for a sandwich beam. In other words, the deflection of the panel in LS-Dyna was compared to that of a similarly supported and loaded beam. According to [14] the total deflection of a symmetrically loaded sandwich can be obtained by superimposing the bending and shear deflections.

In case the beam is homogeneous and isotropic, the bending deflection between the beam's centre ($x=0$) and the support would be

$$y_b(x) = \frac{Pb}{EI}\left(\tfrac{1}{24}x^4 + \tfrac{1}{4}x^2l^2 - \tfrac{1}{2}x^2ll_c\right) \tag{1}$$

where l_c is the distance from the beam midst to the support, l halve of the beam's length, b the beam's width, P the applied pressure, E Young's modulus and I the moment of inertia.

For the non-homogeneous, non-isotropic sandwich plate, an equivalent 'EI' has to be determined. For this classical laminate theory, see e.g. [2], is applied and EI appears to be 2606 [GPa mm^4].

The deflection due to transverse shear load is approximated based on the assumptions that it is completely borne by the honeycomb core and that the shear stress is constant over the core's thickness. With some minor approximations one can derive

$$y_s(x) \approx \int_{x=0}^{l_c} \gamma dx \tag{2}$$

where γ is the shear angle. See also [14]. With

$$\gamma = \frac{\tau}{G}, \tau = \frac{Q}{d}, Q = Px \tag{3}$$

where τ is the shear stress in the core and Q is the transverse force, and one can write for the deflection due to transverse shear load:

$$y_s(x) \approx \int_{x=0}^{l_c} \gamma dx = \frac{Pl_c^2}{2Gd} \tag{4}$$

where G and d are shear modulus and thickness of the honeycomb, respectively.

The deflections y_b and $y_b + y_s$ are shown in Figure 16, together with the deflection as obtained using LS-Dyna.

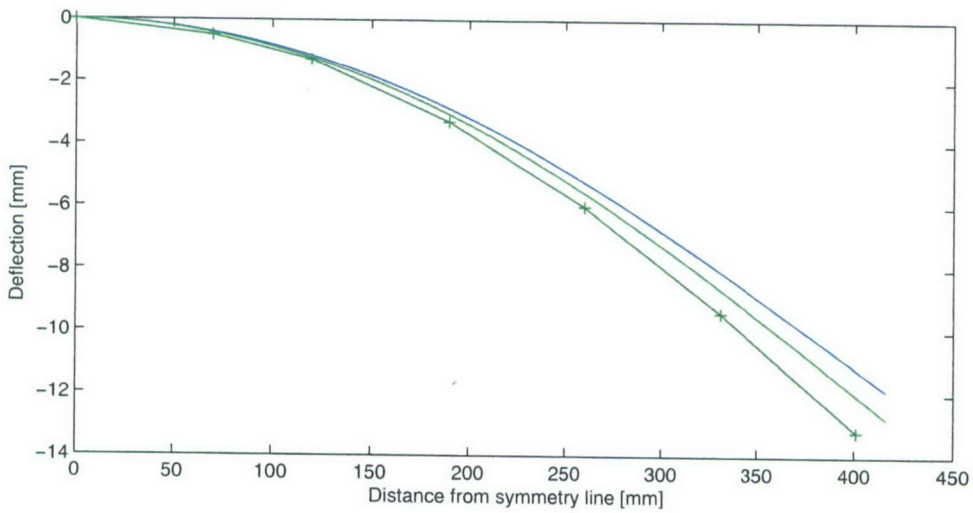

Figure 16 Deflection of sandwich panel, as predicted by LS-Dyna (+ signs) as well as by the analytical equations above, i.e. y_b (upper line) and $y_b + y_s$ (middle line), under a load of 5 [kPa].

This agreement, although not perfect, gives some confidence in the parameters used in the finite element sandwich model. The deviation observed is not caused by the fact that the bending beam equations assume a plane stress situation - which is not the case in plate bending - since this would result in a relatively stiff panel, as compared to the beam. Most probably the differences in implementation of the deflection due to the transverse shear force, rather complex in LS-Dyna and rather simplistic in the present approach, are responsible for the observed deviation.

Failure mechanisms modelled in LS-Dyna

The material model also describes some types of composite failure, i.e. failure of the lamina under tension or compression (no buckling). A Chang-Chang, Tsai-Wu (matrix dominated failure, *Mat_55) or effective strain criterion can be used to calculate failure initiation. Chang-Chang and Tsai-Wu are also distortion energy based criteria.

The material can have some residual strength after failure initiation. Dependent on the type of failure, some of the lamina's elastic properties remain contributing to the element's stiffness matrix, others do not. For example, after tensile matrix failure, Young's modulus in fibre direction E_{11} keeps its original value, whereas E_{22} and the Poisson's ratios v_{21} and v_{12} are set to zero. It is important to note that the neutral axis of the element is *not* updated after break down of one or more lamina.

The failure modes implemented are not useful for the honeycomb core and also delamination between lamina is not modelled.

In the present simulations, *Mat_54 is used, which means that the Chang-Chang model is used for both fibre and matrix dominated failure. Fibres or matrix fail completely if the criterion is reached, i.e. possible plastic strains in these are assumed zero.

6 Simulation Results

One of the LS-Dyna results is the status of the lamina in an element. Five different failure modes, represented by five so-called history variables, can appear for the lamina. They are listed in Table 3 below. If failure has occurred for such mode, the history variable has the value 0, otherwise it has the value 1. History variable 6 represents the status of an element, which can either be intact or failed, where the latter means that all element's lamina have failed completely.

Table 3 Failure modes available in LS-Dyna's *Mat_54-55.

History Variable	Failure mode	Value
1	Tensile fibre mode	1 elastic or 0 failed
2	Compressive fibre mode	1 elastic or 0 failed
3	Tensile matrix mode	1 elastic or 0 failed
4	Compressive matrix mode	1 elastic or 0 failed
5	Effective strain reached	1 elastic or 0 failed
6	Element effectiveness	-1 at least 1 lamina intact or +1 all lamina failed

In the present calculations the criterion for effective strain failure is not specified, i.e. history variable 5 is meaningless. The same holds for variable 6, since no failure criterion is specified for the honeycomb core and the element will thus never fail completely.

N.B. in the simulation the blast load is applied after 1 [ms]. To be able to compare simulation results with experimental results one has to correct LS-Dyna times with -1 [ms]. In the results below the LS-Dyna times are mentioned.

Panel 1 test 1

The simulation of the first test with panel 1 predicts a maximum deflection of roughly 89 [mm], which occurs after 7.5 [ms]. The panel does not release from its supports.

Tensile matrix failure is predicted for Integration Points IP9-IP11, i.e. in the tension loaded layers. Figure 17 shows the locations where this failure has appeared at two stages in the simulation. As will be seen later, this failure doesn't seem to influence the panel's overall behaviour.

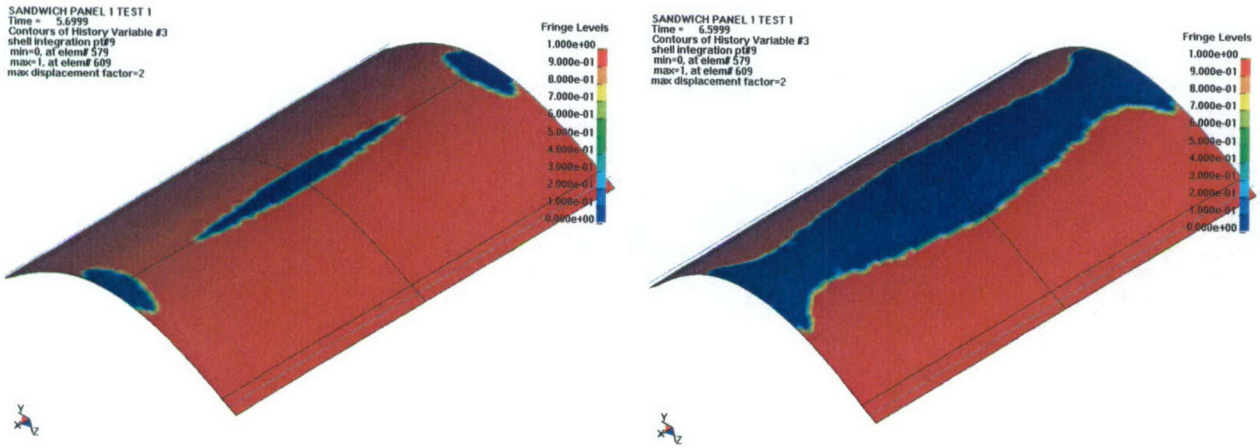

Figure 17 Tensile matrix failure in IP9 after 5.7 and 6.6 [ms], respectively. Red elements are intact, blue element have failed. Other colours are meaningless.

Panel 1 test 2

In the simulation the panel bends globally, folds in the middle and almost simultaneously releases from its supports, at roughly 3.6 [ms].

Table 4 shows the type, time and location of failure as observed in the simulations of test 2. Two values are usually given for 'mode' and 'location', separated by a '/'. The first value in the columns 'mode' and 'location' represent the time and the location of initial failure, respectively. The second value in both columns together show the trend in failure progress. Taking the second row of Table 4 as an example, mode 2 failure initiates in region DE after 3.5 [ms]. After 3.6 [ms], this type of failure has extended into region AE.

Table 4 Failure ordering in panel 1. IP1-IP4 are compression loaded, i.e. they are located at the blast simulator side, IP9-IP12 are tension loaded. IP5-IP8 represent the honeycomb core. Locations according to Figure 18.

Integration point	Orientation	Mode 1	Location	Mode 2	Location	Mode 3	Location	Mode 4	Location	Effect
1		-		3.5/3.6	DE/AE	-		-		
2	45	-		3.5/3.6	DE/AE	-		3.5/3.6	DE/AE	
3	-45	-		3.5/3.6	DE/AE	-		3.5/3.6	DE/AE	
4		-		3.6/3.7	BC/AC	3.7	E'	3.5/3.7	C/AE	' = very local
9		-		3.6/3.7	DE/AE	2.6/3.6	A,E/AE	7.3	A'	' = very local
10	-45	3.5/3.6	DE/AE	-		2.8/3.6	E/AE	-		
11	45	-		-		2.8/3.6	E/AE	-		
12		3.5/3.6	DE/AE	-		3.5/3.6	D/AD	-		

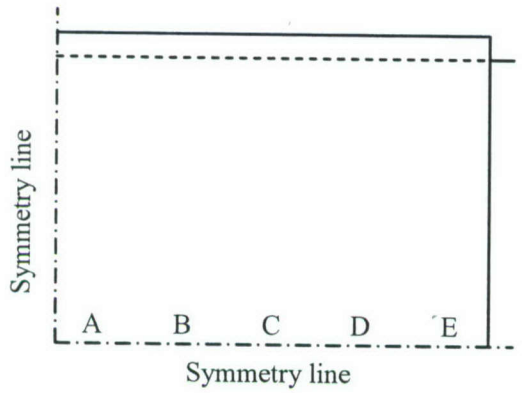

Figure 18 Locations of failure initiation/progress as mentioned in Table 4.

The failure observed in the panel is thus as follows. Firstly tensile matrix failure appears in the tensile loaded facing, between 2.6 and 2.8 [ms]. This does not seem to cause any change in the global behaviour of the plate: no sudden deflections or vibrations occur.

Then, after 3.5 [ms], compression fibre failure appears in IP1-IP4. At the same time tensile fibre failure occurs at IP10 and IP12. In IP9, surprisingly, also compression fibre failure appears. Since it is observed slightly later, after 3.6/3.7 [ms], this is probably due to the dynamic response of the panel to the failure in the other lamina.

Deflection just before primary (i.e. fibre) failure, i.e. at time 3.4 [ms], is about 145 [mm].

In the first graph in Figure 19 some local effects due to fibre failure are seen around the ends of the horizontal centre line. In the second, the very local deformation close to these ends is clearly seen.

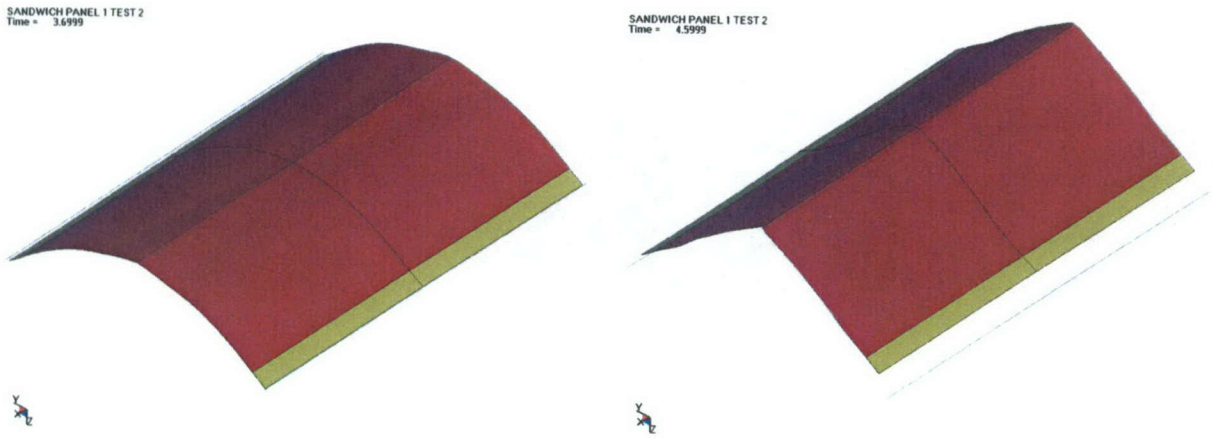

Figure 19 Deflection pattern for panel 1, test 2, after 3.7 and 4.6 [ms].

Panel 2, test 1

In the simulation the panel bends globally, folds in the middle and subsequently releases from its supports around 8 [ms]. See also the sequence in Figure 20.

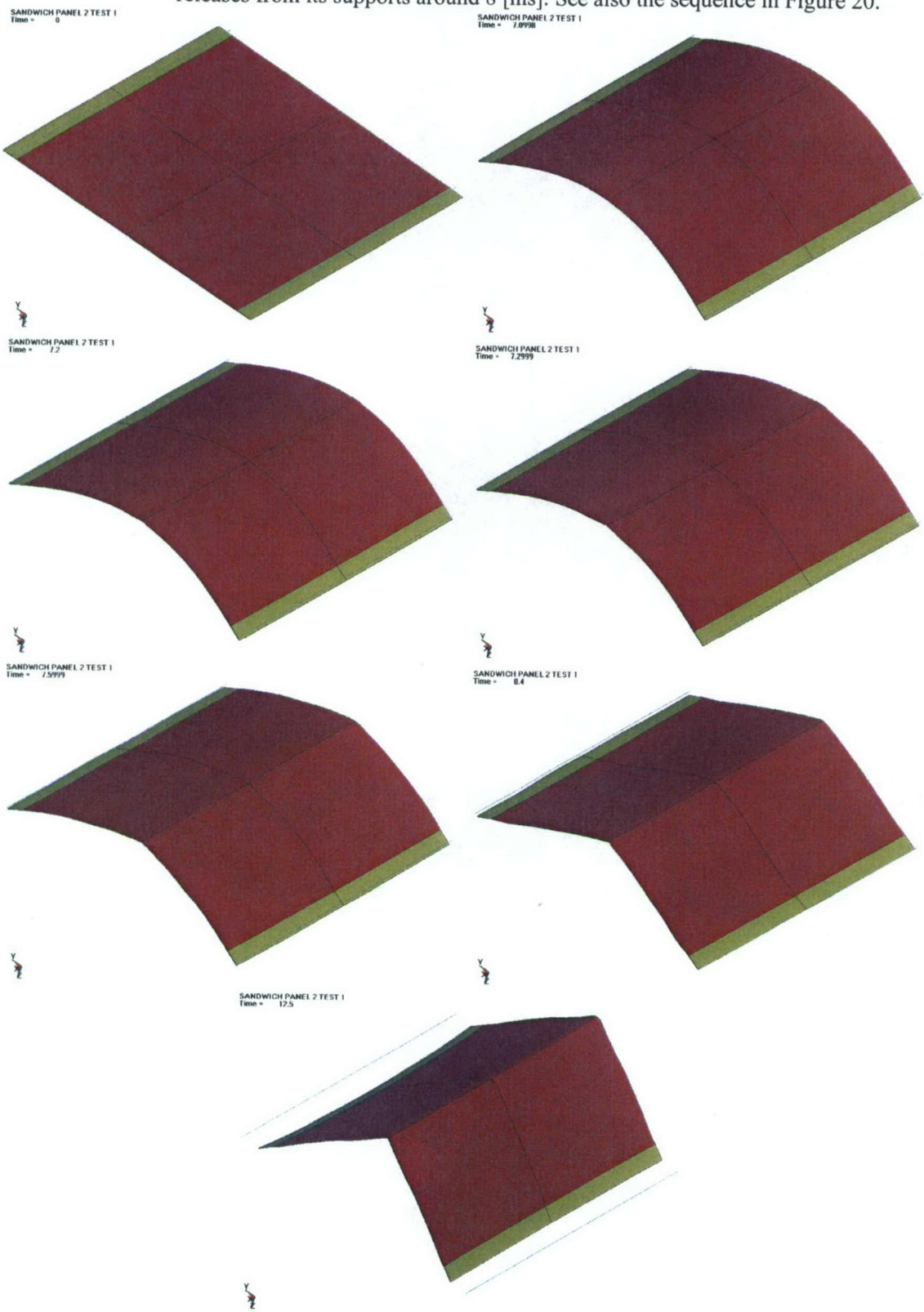

Figure 20.a-g Simulation sequence panel 2, test 1, after 0, 7.1, 7.2, 7.3, 7.6, 8.4 and 12.5 [ms]. N.B. to compare these results with the camera recordings, correct the LS-Dyna times with -1 [ms].

This simulated behaviour agrees almost quantitatively with the experimentally observed behaviour, from Figure 10.
The table below shows the type, time of first appearance and location of failure as observed in the simulations of test 3.

Table 5 Failure ordering in panel 2. IP1-IP4 are compression loaded, i.e. they are located at the blast simulator side, IP9-IP12 are tension loaded. IP5-IP8 represent the honeycomb core. Locations according to Figure 18.

Integration point	Orientation	Mode 1	Location	Mode 2	Location	Mode 3	Location	Mode 4	Location	Effect
1		-		7.2	CD/AE	-		7.6/7.7	A'/E'	
2	45	-		7.2/7.3	CD/AE	7.4	A'/E'	7.2/7.3	DE/AE	' = very local
3	-45	-		7.2/7.3	DE/AE	7.3/7.4	A'/E'	7.2/7.3	CE/AE	' = very local
4		-		7.3	BC/AC	7.2	E/DE	7.3/7.4	BC/AC	
9		8.3/9.7	A/AD	-		4.2/5.3	DE/AE	7.3	BC/AC	
10	-45	7.2/7.3	DE/AE	-		4.9/5.0	E/AE	-		
11	45	8.5/8.6	DE/AE	7.4/7.9	A',E'	4.8/8.5	E/AE	7.4/7.7	A'/E'	' = very local
12		7.2/7.3	DE/AE	-		7.2/7.5	D/AD	7.4	B'	' = very local

The failure observed in the simulation is as follows. Firstly, tensile matrix failure appears in the tension loaded facing, in IP9-IP11, at times ≥4.2 [ms]. This failure does not seem to affect the subsequent panel behaviour, as can be seen in Figure 21, showing the deflection of the panel centre versus time. This is rather surprising; the load bearing capacity of the +45°/-45° lamina is expected to be significantly reduced if the matrix has failed.

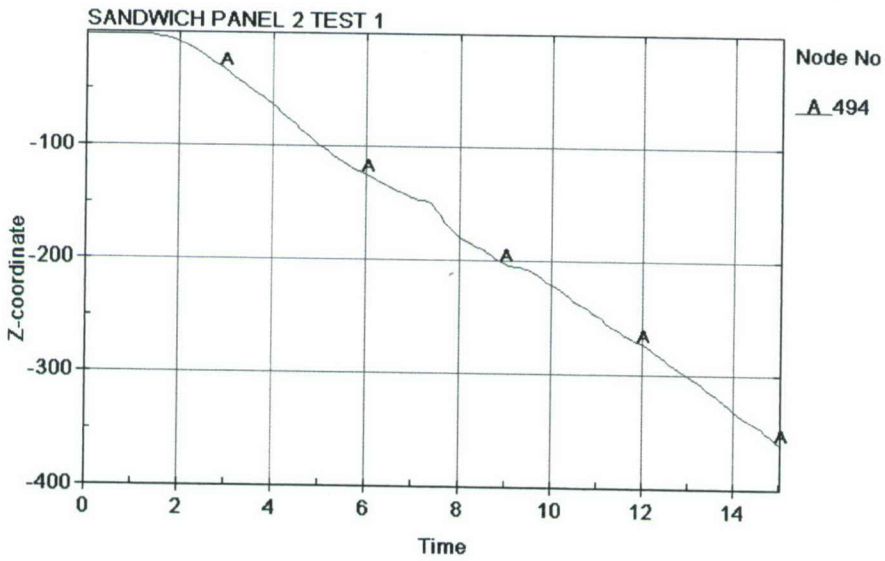

Figure 21 Deflection history of panel centre. Time of fibre failure is visible.

At time = 7.2 [ms] fibre compression failure appears in IP1-IP3, 0.1 [ms] later also in IP4. At the same time, fibre tensile failure appears in IP10 and IP12, surprisingly not in IP11 which is expected to show higher bending strain. This failure does affect the panel's behaviour, the horizontal centre line acts like a hinge and stresses start to relieve.
The deflection just before failure at = 7.2 [ms] is roughly 145 [mm].

7 Analysis

In the following tables the most characteristic markers of the blast process are compared. The times of the LS-Dyna results are corrected with -1 [ms], to account for the delay in load application in the simulations.

Table 6 Panel 1 test 1.

Marker	Experimental	Numerical
Maximum deflection	89	89 [mm]
Time at max. deflection	7.7 [ms]	6.5 [ms]
Failure	None	Tensile matrix failure after 5.2 [ms], but: no effect on the panel's behaviour.

The agreement of the experimental and numerical deflections is remarkable, as is the difference in the times they are reached. The latter as these times match almost perfectly in the last experiment, panel 2, test 1. No effective failure is observed in the experiment as well as in the simulation.

Table 7 Panel 1 test 2.

Marker	Experimental	Numerical
Deflection just before primary failure	143±20 [mm]	145 [mm]
Time at deflection just before primary failure	3.3±0.3 [ms]	2.4 [ms]
Type and location of primary failure	Fibre buckling and fibre tear off at roughly 4/10 of the panel's height.	Fibre compression failure at horizontal centre line of inner facing, fibre tension failure at outer facing.

In this experiment the relation between experiments and numerical simulation is hampered by collision of panel with support's frame and interaction with the safety net.

Table 8 Panel 2 test 1.

Marker	Experimental	Numerical
Deflection just before primary failure	135 [mm]	145 [mm]
Time at deflection just before primary failure	6.3 [ms]	6.2 [ms]
Type and location of primary failure	Fibre buckling roughly at horizontal centre line of inner facing.	Fibre compression failure at horizontal centre line of inner facing, fibre tension failure at outer facing.

In this experiment the agreement in response before the appearance of failure is very good. Given the uncertainty which failure mode is underlying CompositePro's value of the ultimate fibre compression stress, e.g. crushing or buckling, the failure agreement between this experiment and the simulation is remarkable.

The fact that failure in the outer facing appears in the simulation but not in reality may be due to the fact that LS-Dyna does not update the neutral axis of an element after one or more of its lamina have failed. In reality, however, this does happen; apparently buckling of the inner facing occurs first and after buckling of this inner facing and local crushing of the honeycomb, the outer facing functions as a hinge and apparently can survive the resulting bending radius. The fact that tension and compression fibre failure occur at the same time in the analysis may also be due to the output interval chosen in the calculation, i.e. 0.1 [ms].

Generally, it is quite remarkable that simulations characterized by:
1 the use of a rather arbitrary - i.e. not tested on lamina - failure criterion;
2 and the use of literature values for carbon fibre reinforced epoxy lamina;
give a reasonable indication of the blast performance of honeycomb sandwich structures, at least for relatively low blast loads (panel 1, test 1 and panel 2, test 1).

The agreement in the case of failure, panel 2 test 1, is thanks to the fact that the loaded facing appears decisive for the failure under relatively low blast loads, rather than the shear strength of the honeycomb or its interface with the facings, as initially expected.

8 Input data for CFRP panel

8.1 Selection of composite material

The composite material to be modelled should be a material used for helicopters or otherwise a composite used in the aircraft structures. For budget reasons a choice could be made between four different carbon fibre-reinforced composite materials, because ballistic results were already available for these from previous studies. In consultation with the project leader the Hercules AS4/3501 provided by DERA [3] as chosen. The main reasons were that for the first simulation trial the material should be a single flat material (no honeycomb structure or blade-stiffened panel) and that the post-mortem plates were still available for material testing.

8.2 Material input parameters for AS4/3501 composite

To simulate a composite material it is critical to know most of the material parameters like engineering constants and failure criteria. Otherwise the unknown input parameters are 'tuned' to correlate the simulation result with the experimental result. The Hercules AS4/3501 composite plates were defined by DERA/Farnborough [3]. It is a woven carbon fibre (AS4) reinforced (3501 is an epoxy matrix material) panel. The plates have a large range of thicknesses between 3.2 and 25.4 mm. Except for the type of fibre and matrix material no material parameters are known.

Therefore, all material input parameters (see Table 1) still have to be determined. However, it is not possible to fabricate test samples, because the material build-up (orientation direction of the fibres), fibre/matrix ratio and fabrication process are not known. Since the post-mortem panels were available, these could be used to get test samples for material testing. This limits the material tests which can be performed, because the number of test samples is limited and not all test sample types could be made from the post-mortem plates. This is explained in the following paragraph. While examining the composite plates they appear to have a transversal-isotropic orientation [0°/90°/±45°]. This means that the plain weave layers are laid in two different orientations, layers with fibres in 0°/90° direction and layers turned 45°. Because not all input parameters could be determined a brief literature survey has been performed to collect as much data as possible on this type of composite.

Table 1 gives an overview of the material input parameters needed for the ADAMMO [4] model and the determined material parameters from tests or from literature. The material properties are assumed to be the same in tension and compression. The ADAMMO model has the possibility to include non-linear curves. The required input parameters for this feature (Strength; orthotropic yield) are not included in Table 1, because the CFRP panels show a linear stress strain curve [3] (according to Hooke's law).
The material tests will be briefly discussed in the following paragraph. Further details of the material characterization tests and their results are given in a separate report.[5]

Table 9 Material input parameters for AS4/3501 $[0°/90°/\pm45°]_n$, with x and y the fibre directions, and z the thickness direction, * values are determined from the post-mortem panels.

Input parameter Material parameters		Value / input	Source / Test
Density	ρ	1.58 g/cm^3	[6]
Youngs Modulus x	E_x	44.9 GPa*	[5] 0° tension test
Youngs Modulus y	E_y	44.9 GPa*	[5] 0° tension test
Youngs Modulus z	E_z	11.7 GPa	[7], [8]
Poisson ratio xy	ν_{xy}	0.311*	[5] 0° tension test
Poisson ratio yz	υ_{yz}	0.33	[7]
Poisson ratio zx	υ_{zx}	0.31	[7]
Shear Modulus xy	G_{xy}	17.6 GPa*	[5] 45° tension test
Shear Modulus yz	G_{yz}	3.57 GPa*	[5] V-notch beam method
Shear Modulus zx	G_{zx}	3.27 GPa*	[5] V-notch beam method
Volumetric respons	EOS	linear	Assumed linear; should be determined form a flyer plate impact test
Failure criteria			
Tensile Failure Stress x	F_x	431 Mpa*	[5] 0° tension test
Tensile Failure Stress y	F_y	431 Mpa*	[5] 0° tension test
Tensile Failure Stress z	F_z	25 MPa	[9]
Maximum Shear stress xy	F_{xy} (= τ_{xy})	247 MPa*	[5] 45° tension test
Maximum Shear stress yz	F_{yz} (= τ_{yz})	28.2 MPa*	[5] V-notch beam method
Maximum Shear stress zx	F_{zx} (= τ_{zx})	33.3 MPa*	[5] V-notch beam method
Fracture Energy xx		0	[5] Remaining energy after failure in 0° tension test
Fracture Energy yy		0	[5] Remaining energy after failure in 0° tension test
Fracture Energy zz	G_{Ic}	100 J/m^2	[10] Mode I delamination
Fracture Energy xy		580 J/m^2	[11] assumed as Mode II failure [4]
Fracture Energy yz	G_{IIc}	580 J/m^2	[11] Mode II failure
Fracture Energy zx	G_{IIc}	580 J/m^2	[11] Mode II failure

8.3 Material characterization tests

In this paragraph a short review of material characterization tests is given, including explanations for tests which could not be done. Details of the performed material characterization tests are given in [5].

8.3.1 Tension test

In the tension test according to standard ASTM D3039 the specimen is loaded in the main fibre directions. The CFRP panels were build-up from plain weave layers and thus each layer behaves orthotropic. Since the laminate is build up from $0°/90°/\pm45°$ layers, the whole laminate is orthotropic. For these materials it can be assumed that the material parameters in the main (fibre) directions x and y are the same.
The following parameters can be determined from the 0° tension test according to standard ASTM D3039: E_x, F_x, ν_{xy}, E_y, F_y and ν_{yx}.
For determination of these parameters in thickness (z) direction, no commonly accepted standard methods are available. The methods used give no consistent results.
Engineering constants often are determined theoretically from fibre and matrix parameters using the classic laminate theory. In two references theoretical determined values of the E_z,, ν_{xz}, and ν_{zy} were found for a similar composite. Because they show almost the same values, these were used as a first estimate and listed in Table 1.

8.3.2 *Shear tests*

For the determination of shear properties different test methods are available. Two different test methods were used to determine all six parameters, which is illustrated in Figure 1.

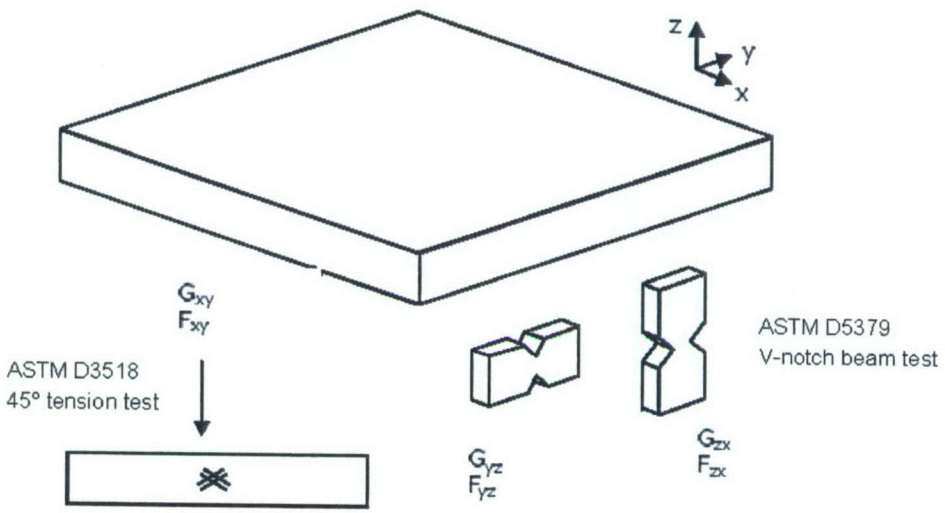

Figure 22 Illustration of test samples for shear tests.

The in-plain shear values (G_{xy} and F_{xy}) are determined according to standard ASTM D3518. This method is almost equal to ASTM D3039, only in this test the specimen is loaded in 45° direction of the main fibre direction. With this method the modulus and strength can be easily calculated from the results. Disadvantage of this method are the higher strength values for thicker test samples. For conservative values it is recommended to use thin test samples.

The V-notch beam test according to ASTM D5379 can be used to determine the shear properties in the other directions (G_{yz} , F_{yz} and G_{zx} ,F_{zx}). This test method can determine the strength and modulus. The disadvantage is the complex geometry of the test samples, which have to be accurate. Fortunately it was possible to manufacture the test samples from a thick (25 mm) panel.

The results are listed in Table 1.

8.3.3 *Fracture toughness test*

Fracture toughness tests are needed for the fracture energy input parameters of the ADAMMO model. [4] These parameters are mainly responsible for damage in the simulation. So for accurate damage modelling it is important to use these failure criteria.

To guarantee good test results the samples need an accurately defined delamination before testing. Normally the test samples are manufactured for this test specifically with a thin Teflon foil between, to create the defined delamination. From the post-mortem plates it is impossible to create this defined delamination. So no test samples are available for this test.

Because these parameters are important for a simulation, a lot of effort has been made to find fracture toughness data for this material. The data found, is not explicitly for orthotropic AS4/3501:

- G_{Ic} in Table 1 was found for T300/epoxy and Type II CF/epoxy;
- G_{IIc} in Table 1 was found for unidirectional AS4/3501.

Therefore the values mentioned in Table 1 for the fracture toughness are a first estimate. If damage in the model does not correspond with the damage shown in the C-scan results, these are the parameters to be adjusted.

9 Simulation of the CFRP panels

The Hercules AS4/3501 composite plates were tested against three sizes of a fragment simulating projectile (FSP): 1.1 gram, 2.85 gram and 5.3 gram. This is done for five different thicknesses of approximately 3.5, 7.1, 10.2, 14.3 and 17 mm. All these results are reported in PML 1999-B023 [3]. In the given timeframe it is not possible to simulate all ballistic tests, so two test configurations were chosen to be simulated: 3.5 mm and 14.3 mm against 1.1 gram FSP. The ballistic data is given in Table 2. A C-scan is made of the 14.3 mm panel, which is used for the 1.1 gram FSP test.

Table 10 Ballistic data from tests [3].

Filename:	V_{impact} (m/s)	$V_{residual}$ (m/s)
Thickness = 3.5 mm		
Impact1	848	728
Impact2	619	526
Impact3	266	201
Thickness = 14.3 mm		
Impact1-thick	822	370
Impact2-thick	698	270
Impact3-thick	597	155

9.1 Basic set-up of the simulations

All simulations are performed with Autodyn version 5.0.2a in 3D. The basic set-up is shown in Figure 2. Because of symmetry, only a quarter of the actual problem is modelled.

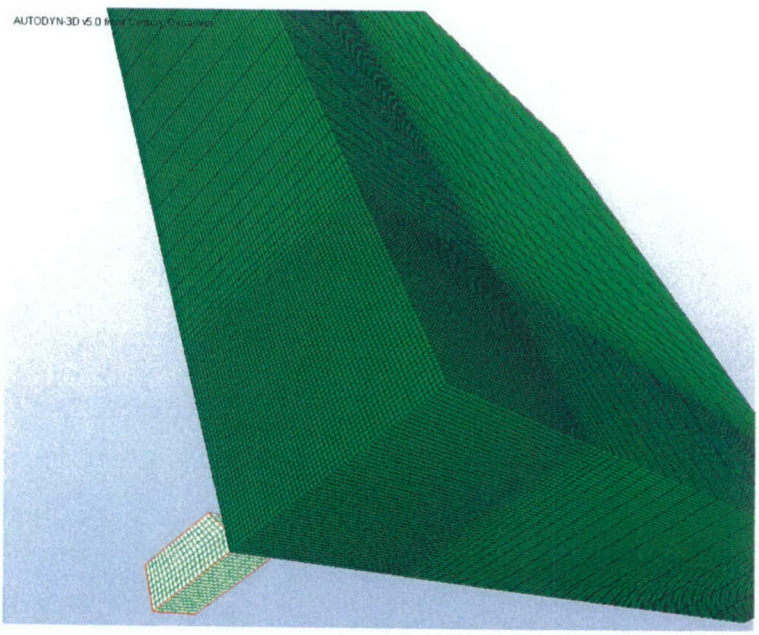

Figure 23 Basic set-up of the simulations (in this case the thick target is shown).

As can be seen in Figure 2, the dimension of the grid of the target gradually expands when one moves away from the hit area. In Table 3 the grid characteristics for the two

different target sizes are summarised. A transition boundary condition is applied on the lateral edges of the target to simulate a target of infinite length and height. This boundary condition transmits stress waves through the boundary instead of reflecting them.

Table 3 Characteristics of the grid of the two targets.

	Thin target (3.5 mm)	Thick target (14.3 mm)
Length (mm) x Height (mm)	100 x 100	75 x 75
# Cells (length) x # cells (height)	100 x 100	70 x 70
# Cells in thickness direction	14	57
# Total cells	140000	279300
# Small cells within target area	60 cells of 0.25 x 0.25 x 0.25 mm^3	50 cells of 0.25 x 0.25 x 0.25 mm^3

A close-up of the geometry of the modelled 1.1 gram FSP is shown in Figure 3. The model consists of 1600 elements with an average size of approximately 0.32 x 0.32 x 0.32 mm^3.

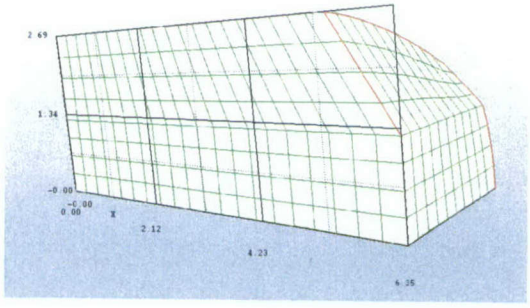

Figure 24 Geometry of the modelled 1.1 gram FSP.

The material of the FSP is modelled with a shock equation of state and an elastic strength model of steel. Since the FSP does not deform during the impact, this is sufficient. The used parameters are:

Gruneisen gamma = 2.17
C1 (sound velocity) = 4569 m/s
S1(shock parameter) = 1.49
G (Shear modulus) = 81.8 GPa

9.2 Results regarding residual velocity

With the input parameters from Table 1, the results as shown in Table 4 are obtained.

Table 11 Ballistic data from tests [3] and the results from the Autodyn models.

Filename:	V_{impact} (m/s)	$V_{residual}$ (m/s) experimental	$V_{residual}$ (m/s) from Autodyn
Thickness = 3.5 mm			
Impact1	848	728	688
Impact2	619	526	495
Impact3	266	201	205
Thickness = 14.3 mm			
Impact1-thick	822	370	350
Impact2-thick	698	270	270
Impact3-thick	597	155	194

When the experimental results are compared to the Autodyn results, one should keep in mind that the experimental results are from one experiment only. Experimental results have a spreading of approximately 10 m/s.
As one can see, the results are consistent with the results obtained from experimental data. However, further improvements could be made if more material parameters are determined by material testing, see Table 1 and paragraph 'sensitivity study parameters'. Also flyer plate experiments could be done to determine the shock equation of state of this material.

9.3 Results regarding damage of target

To compare the damage from the output of the Autodyn model to the damage which is present in the real target, a C-scan is made of the 14.3 mm thick post-mortem target. The results of the C-scan are shown in Figure 4. More details about the C-scan can be found in the report from ALE [5].

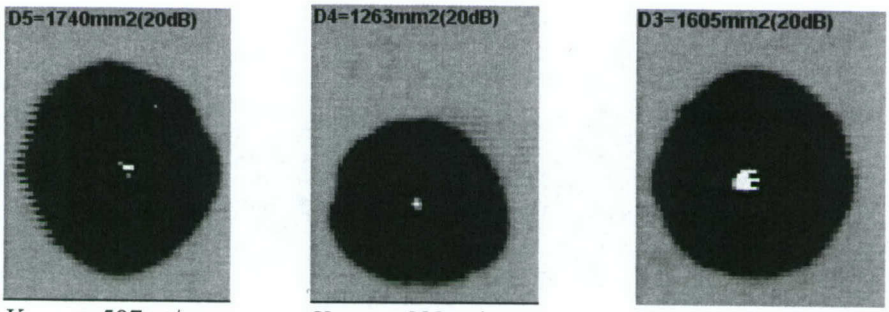

Figure 25 C-scan results for the three different shots. The black area indicates damaged material. The number above each picture indicates the area of damaged material (the white area is the penetration channel). R_{damage} is the 'average' radius of the damaged area.

The C-scan shows that the higher the impact velocity, the less damaged material is visible. Nevertheless, the differences are small and more post-mortem panels should be analysed before the final conclusions can be drawn.
To compare the C-scan results directly with the Autodyn simulations, a transparent damage plot is created in Autodyn. These can be seen on the left hand side of Figure 5. Overall, it seems that the damage is in the same order of magnitude as observed in the real C-scan. However, a few comments should be made. First, the red area visible in Figure 5, is the area in which the material is more than 60% damaged. It is hard to say which percentage of damage leads to the black area in the real C-scan. Maybe it is better to compare cross-sections of the material, which are shown on the right hand side of Figure 5. Nevertheless, no cross-sections of real post-mortem targets are available. Secondly, in the simulations it seems that the higher the impact velocity, the more damaged material is visible. This is not the case in the real C-scans. It is possible that this is caused by the shockwaves in the simulation, because the higher the impact velocity, the greater the intensity of the shockwaves. However, the correct material parameters to describe shock transmission are not available for this material. Therefore, the shock waves could have a greater influence in the simulation than in reality. Finally, as can be seen in the right hand side of Figure 5, the projectile is not even half way up the target yet. Nevertheless, the velocity of the projectile is already constant.

However, it is possible that the damage still grows a little bit further. But because of time limitations of this project it was not possible to run the simulations for a longer time. It so happens that the run time of the simulation grows extensively as the simulation moves to the end, because the cells are heavily distorted and the time-step for each cycle becomes smaller.

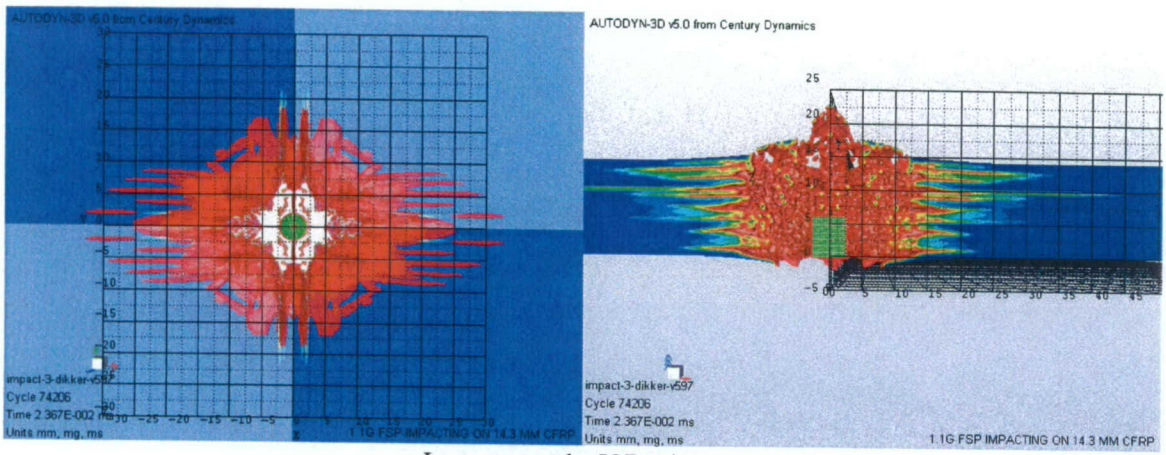

Impact speed : 597 m/s

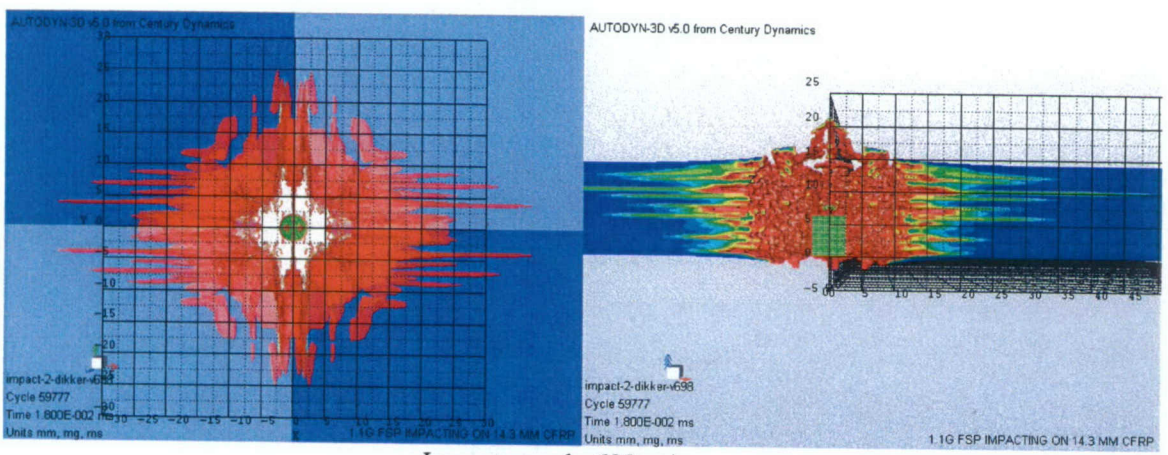

Impact speed : 698 m/s

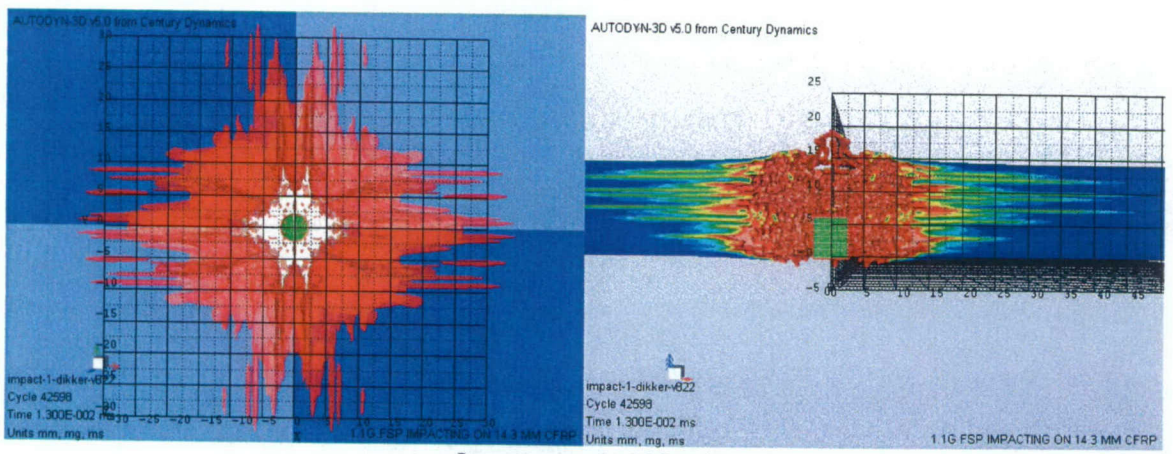

Impact speed : 822 m/s

Figure 26 Left: 'C-scan' made with Autodyn for the three different impact speeds (14.3 mm target) *Right: Cross-section of damaged material (14.3 mm target).*

9.4 Sensitivity study parameters

Because of budgetary and time limitations only three (sets of) parameters could be varied with only one target and one velocity. The simulation which ran the fastest is chosen as reference simulation. This was the thin (3.5mm) target with a velocity of 848 m/s.
The parameters which are varied are summed up in Table 5. Only one (set of) variable is varied each simulation, while the other parameters were kept constant as in Table 1. The parameters below are chosen, because these where some of the parameters which are not determined from material testing.

Table 12 The three (sets of) parameters which are varied as sensitivity study.

Parameter	Symbol	Original value	Other values modelled	Indicated in legend as:
Tensile Failure Stress z	F_z	25 MPa	1.10^{20} (never failure)	No failure in z-direction
Fracture Energy zz	G_{Ic}	100 J/m^2	500 J/m^2 1000 J/m^2	Fract. Energy zz: 5x/10x higher
Fracture Energy xy		580 J/m^2	5800 J/m^2; 58000 J/m^2	
Fracture Energy yz	G_{IIc}	580 J/m^2	5800 J/m^2; 58000 J/m^2	Fract. Energy shear: 10x/100x higher
Fracture Energy zx	G_{IIc}	580 J/m^2	5800 J/m^2; 58000 J/m^2	

In Figure 6 the results are shown for the velocity of the FSP as a function of time. The influence of the variation of the parameters on the residual velocity of the FSP is very small. Varying the fracture energy in the shear directions has no influence at all on the residual velocity. Changing parameters in the through thickness direction (z-direction) has a small influence, varying the residual velocity with a maximum of 8 m/s.

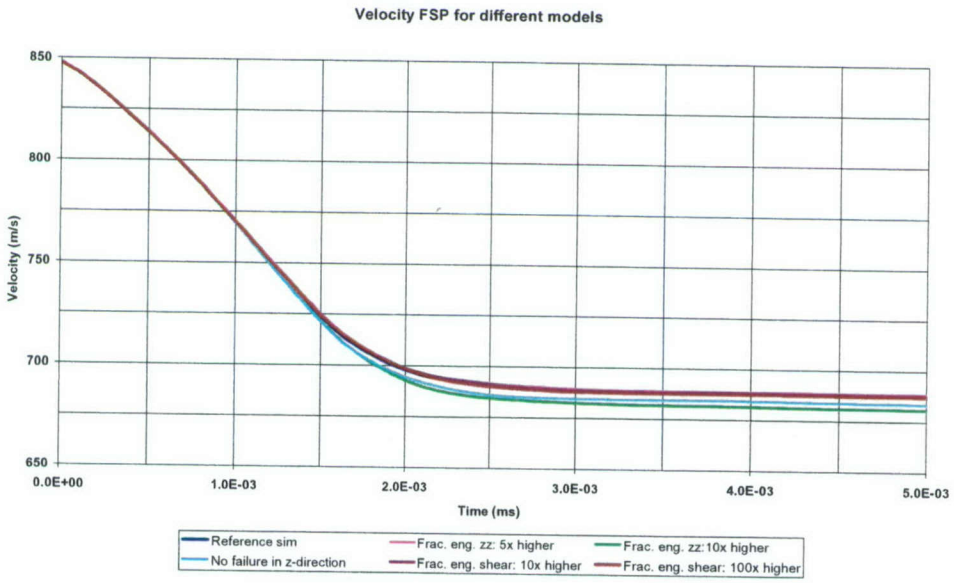

Figure 27 Velocity FSP as function of time for the different parameters.

The influence on the occurrence of damage is also small for the fracture energy in the shear direction. This can be seen in Figure 7. In this figure the damage in the xz-direction is visualized in a cross-section for the different parameters. The difference in

damage does occur when varying the parameters in the through thickness direction (z-direction).

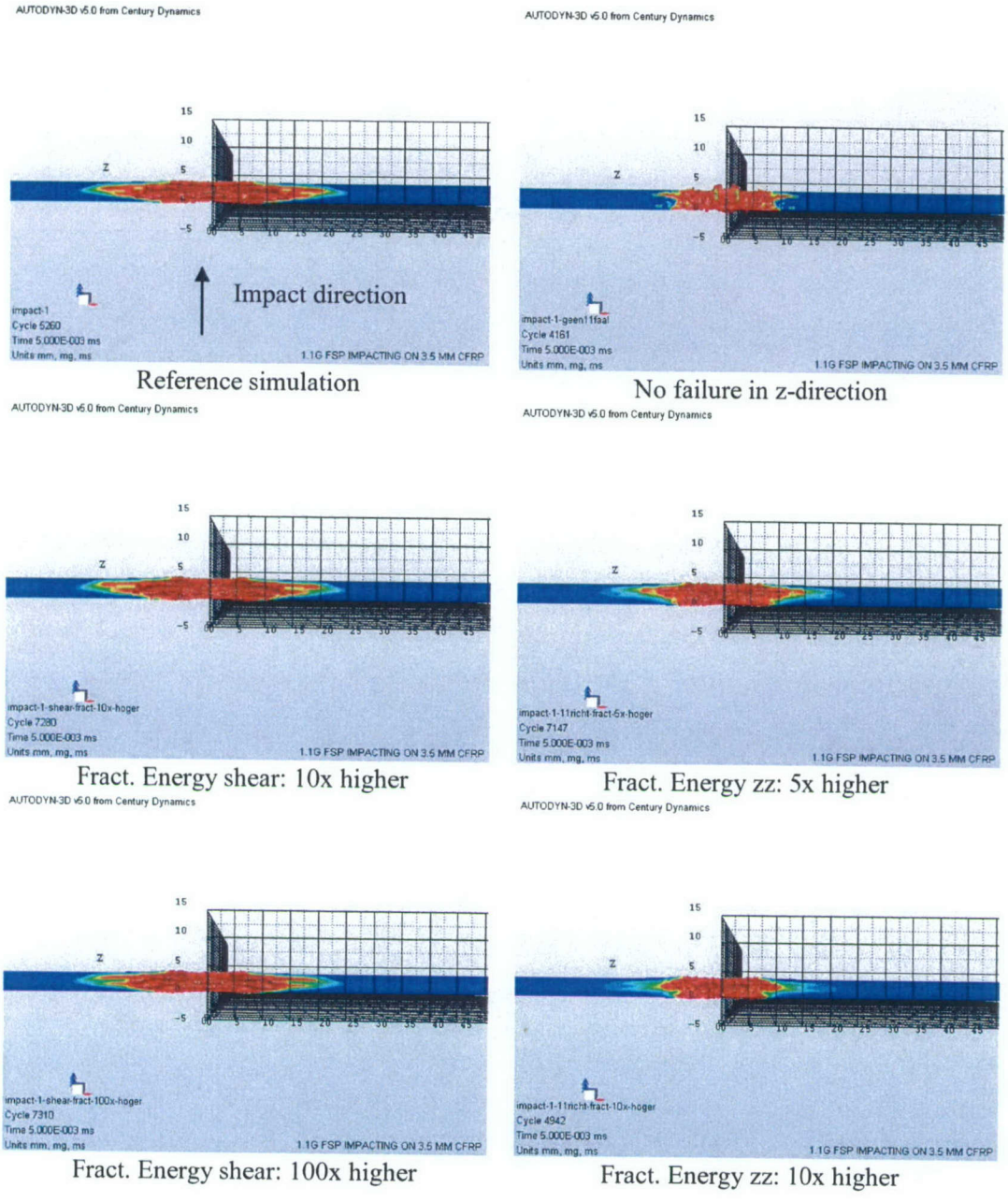

Figure 28 Variation in damage for the different parameters.

A comment should be made that the damage is compared at 5 μs after impact of the FSP. As can be seen in Figure 6, after 5 μs the FSP is not slowed down anymore by the target. Nevertheless, the damage in the target does still get larger after 5 μs. Therefore, this is not the final damage that will occur in the panel. However, for time reasons 5 μs is chosen for comparison.
To compare the difference between this damage and the final damage two simulations have been run further. The result is shown in Figure 8.

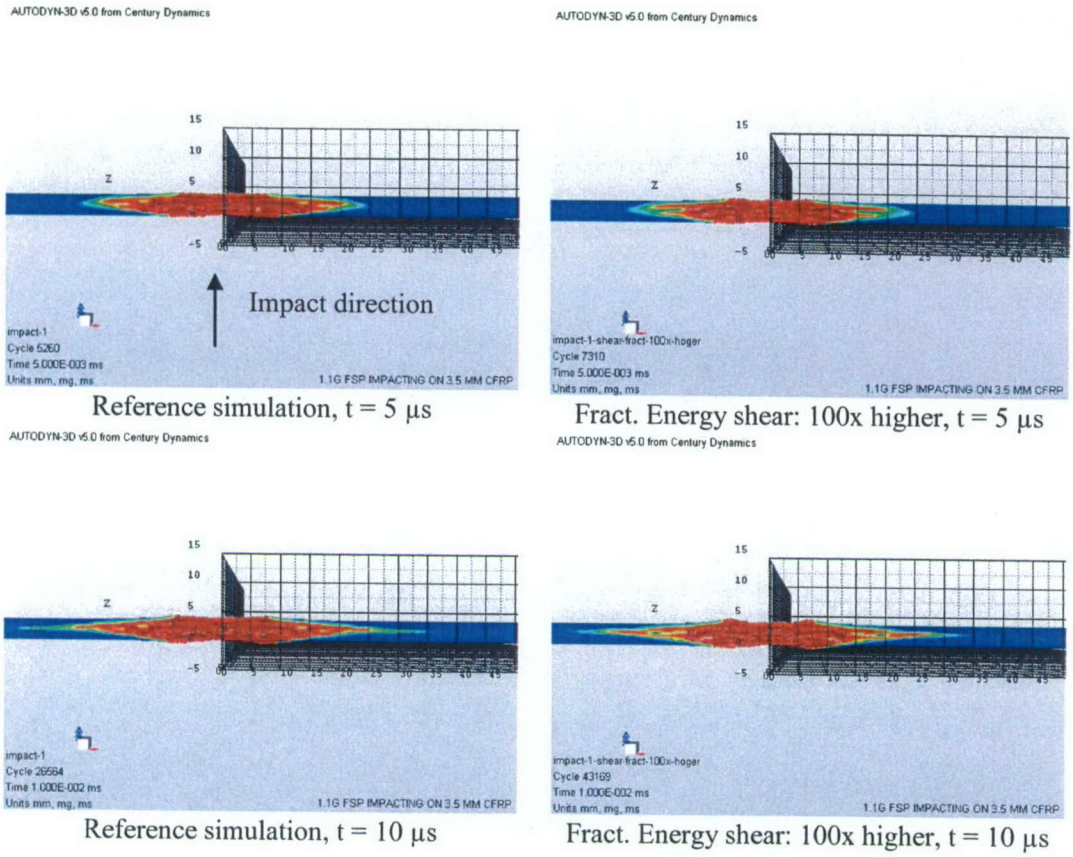

Figure 29 Comparison between damage at 5 and 10 µs after impact for the reference simulation and for the simulation with a different fracture shear energy.

Out of Figure 8 one can conclude that there is a significant difference in damage between 5 and 10 µs after impact. Nevertheless, the difference between the two different simulations remains negligible. Therefore, the conclusion is drawn that the differences shown in Figure 7 are also expected in the final damage of the panel.

10 Conclusions and recommendations

A studies was performed on the effect of fragment impact and blast loading on composite helicopter structures. For both the blast and fragment study finite element simulations methods were worked out. Material parameters necessary as imput for the simulations were obtained from small scale experiments and from literature. A lange scale blast experiment was performed to validate the numerical results.
The fragment impact simulation is validated using data from previous experiments and from C-scan results.

The following conclusions were drawn from the blast and fragment studies:

Blast effect on a helicopter sandwich panel
For relatively low blast loads sandwich failure is dominated by fibre buckling in the blast loaded facing. It is important to note that this conclusion is based on just one experiment (panel 2, test 1).

For the lowest blast loads, the finite element simulations performed were quite successful in the sense that numerical and experimental results agreed reasonably (panel 1, test 1) to well (panel 2, test 1).

The agreement in time, type and location of sandwich failure (panel 2, test 1) is thanks to the fact that the loaded facing appears decisive for the failure under relatively low blast loads, rather than the shear strength of the honeycomb or its interface with the facings, as initially expected.

The question to be answered in future work is if the compressive failure of the loaded facing is also decisive in common helicopter sandwich structures, under more realistic boundary conditions.

This is not necessarily true, as indicated by the experiment with the highest blast load (panel 1, test 2). Although there are too many uncertainties in the performed experiment to draw reliable conclusions with respect to the cause, honeycomb failure is significant in this panel.

A conclusion which has to be made here, too, is that the use of high speed camera recordings is of great help in:
1 interpreting the finally observed blast effects;
2 comparing the specific times and locations at which failure occurs;
3 as a results of the former point, verification of the finite element modelling.

Also the safety net seems useful in preventing damage caused by other means than the blast load. However, given the remains of the net after test 2 on panel 1, panel loads by the net might be significantly, something to pay attention to. Perhaps a more compliant net could help.

The comparison of experimental and numerical results is hampered by the observed collisions between the sandwich panel and the mounting frames of the supports. For future test the mounting frame of the supports should therefore be adapted to prevent the panel from colliding with these frames.

Fragment impact on a composite panel

A finite element model of the CFRP AS4/3501 has been made with the use of the software Autodyn v5.0.02a in 3D. The parameters which are used in this model are partly derived from material tests and partly from data found in the literature for similar composite materials. With this finite element model it is possible to determine the residual velocity of an impacting projectile and to determine the damage inside the composite target.

With the finite element model impact simulations are made with a 1.1 gram FSP against two different targets, 3.5 mm and 14.3 mm thickness. The residual velocities of the simulations are consistent with the residual velocities measured at the experiments.

In order to compare the damage from the simulations to the damage inside the real panel, C-scans are made of the 14.3 mm post-mortem target. The damage observed is in the same order of magnitude as in the simulations. Nevertheless, the trend that more damage is observed with a lower impact velocity is not visible in the simulations. In the simulations this is probably caused by the transmission of shock waves, because the higher the impact velocity, the greater the intensity of the shock wave. Therefore, the parameters which describe the transmission of shock waves in the material should be determined by flyer plate tests.

Another reason could be that the simulations should run longer in time. It is possible that the extra damage at lower impact velocities occurs later in time. However, more research is necessary to resolve this problem.

Out of the sensitivity study the conclusion can be drawn that also the material properties in the through thickness direction should be determined. The influence on the residual velocity of the FSP is very small. Nevertheless, the influence on the occurrence of damage is significant. The fracture energy parameters in the shear directions are of very little influence on the final result of the simulations. This applies to both the residual velocity of the FSP and the occurrence of damage.

12 Signature

Rijswijk, March 2005

TNO Defence, Security and Safety

A. Schilt
Group leader

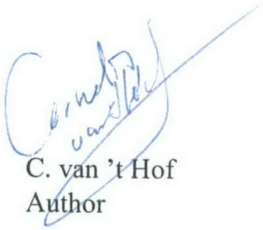

C. van 't Hof
Author

K. Herlaar
Author

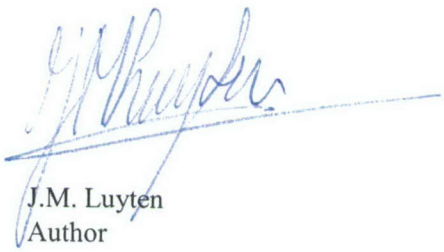

J.M. Luyten
Author

M.J. van der Jagt
Author

A Drawing of sandwich panel

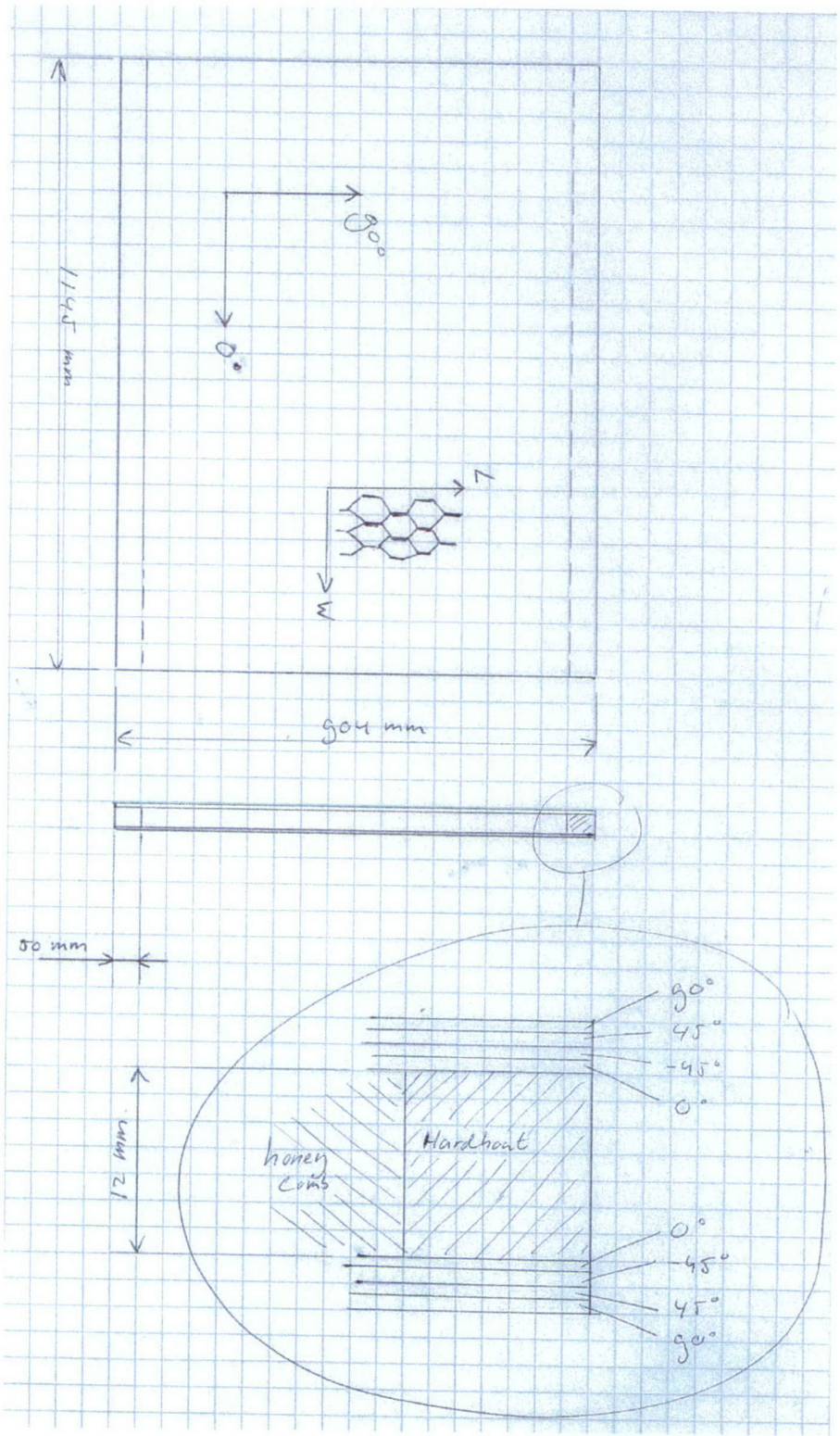

Figure A.1 Drawing of sandwick panel for blast test.

B Material Data

The material data as used in LS-Dyna's *Mat_54-55 are summarized below.

Table B.1 Indicatory values for carbon reinforced epoxy lamina properties, as obtained from CompositePro.

Property	Value	Unit
Young's modulus 1-direction	1.448E+11	[Pa]
Young's modulus 2-direction	9.655E+09	[Pa]
Young's modulus 3-direction	9.655E+09	[Pa]
Shear modulus 12-direction	5.862E+09	[Pa]
Shear modulus 13-direction	5.862E+09	[Pa]
Shear modulus 23-direction	3.462E+09	[Pa]
Poisson's ratio υ_{12}	2.500E-01	[-]
Poisson's ratio υ_{13}	2.500E-01	[-]
Poisson's ratio υ_{23}	4.065E-01	[-]
Tension strength 1-direction	2.172E+09	[Pa]
Tension strength 2-direction	5.378E+07	[Pa]
Shear strength 12-direction	8.676E+07	[Pa]
Compression strength 1-direction	-1.723E+09	[Pa]
Compression strength 2-direction	-1.612E+08	[Pa]
Max. strain 1-direction	1.500E-02	[-]
Max. strain 2-direction	5.570E-03	[-]
Max. shear strain 12-direction	1.480E-02	[-]
Min. strain 1-direction	-1.190E-02	[-]
Min. strain 2-direction	-1.670E-02	[-]
Density	1.578E+03	[kgm^{-3}]

Table B.2 Indicatory values for honeycomb properties, as obtained from www. HexcelComposites.com, and assumptions. Values obtained from www.HexcelComposites.com are indicated by 'HC'. Assumed values were indicated by an 'A'.

Property	Value	Unit	Source
Compression modulus (T-direction)	140	[MPa]	HC
Compression strength (T-direction)	2.4	[MPa]	HC
Shear modulus L-direction	40	[MPa]	HC
Shear strength L-direction	1.2	[MPa]	HC
Shear modulus W-direction	25	[MPa]	HC
Shear strength W-direction	0.7	[MPa]	HC
Density	48	[kgm^{-3}]	HC
Young's modulus 1-direction (less relevant)	1	[MPa]	A
Young's modulus 2-direction (less relevant)	1	[MPa]	A
Shear modulus 12-direction (less relevant)	1	[MPa]	A
Poisson's ratio υ_{21} (less relevant)	0.3	[-]	A

Table B.3 Used wood properties from [12]. N.B. Longitudinal means parallel to the fibre, radial and tangential mean normal and tangential to the growth rings, respectively.

Property	Value	Unit
Young's modulus longitudinal (i.e. 1-) direction	11	[GPa]
Young's modulus tangential (i.e. 2-) direction	0.902	[GPa]
Shear modulus LT-direction	0.891	[GPa]
Shear modulus RT-direction (R=radial)	0.979	[GPa]
Shear modulus LR-direction	25	[GPa]
Density	720	[kgm^{-3}]
Poisson's ratio υ_{21}	0.033	[-]

C Photographs of Blast Test

Pictures of damage of panel 1 after test 2.

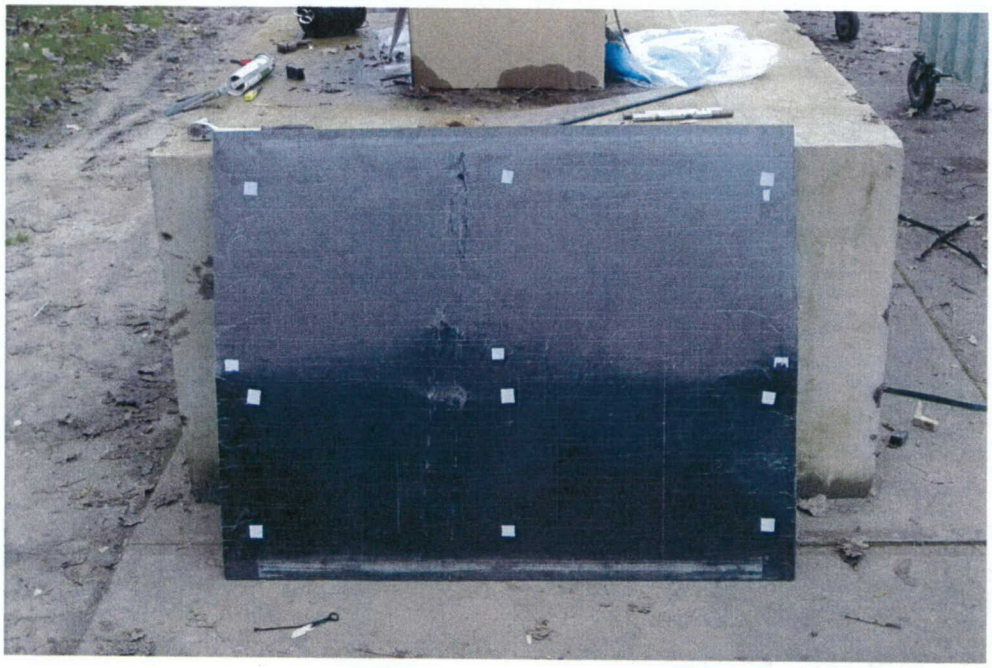

Figure C.1 Unloaded panel side with large indentation by the chain used to tighten the safety net.

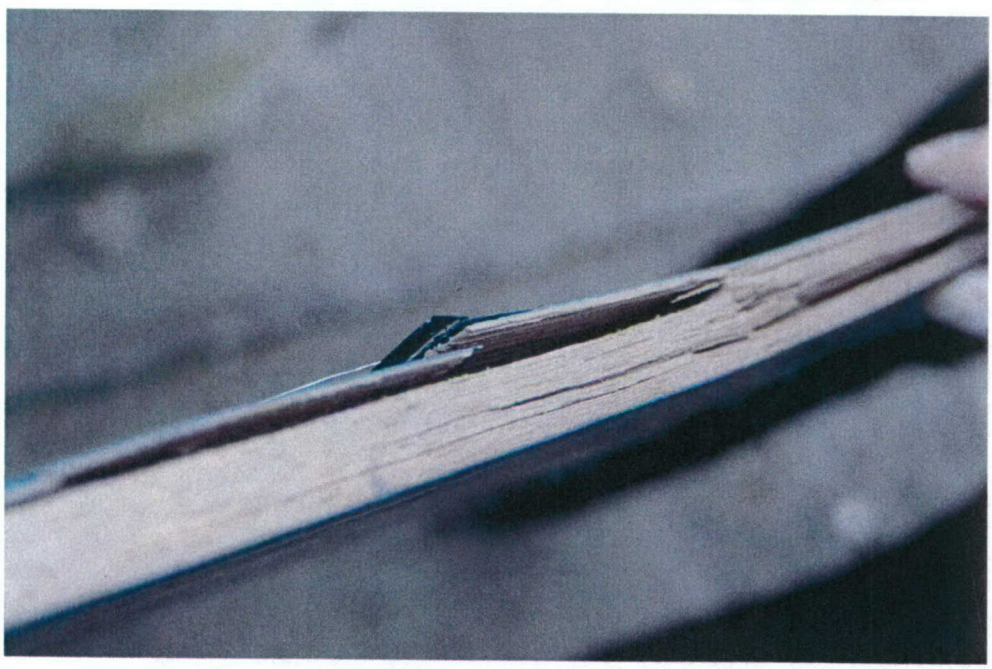

Figure C.2 Delaminated wooden insert and teared facing.

Figure C.3 Side of panel 1 after test 2. From left to right, the details follow in in the Figure C.4 to Figure C.7 below

Figure C.4 Severely damaged honeycomb core and teared facings at the end of the main fold (1). Note the green fibres, which are remains of the safety net.

Figure C.5 Severely damaged honeycomb core and teared facings at the end of the main fold (2). Note the green fibres, which are remains of the safety net.

Figure C.6 Severely damaged honeycomb core and teared facing (3).

Figure C.7 Delaminated wooden insert and intact facing.

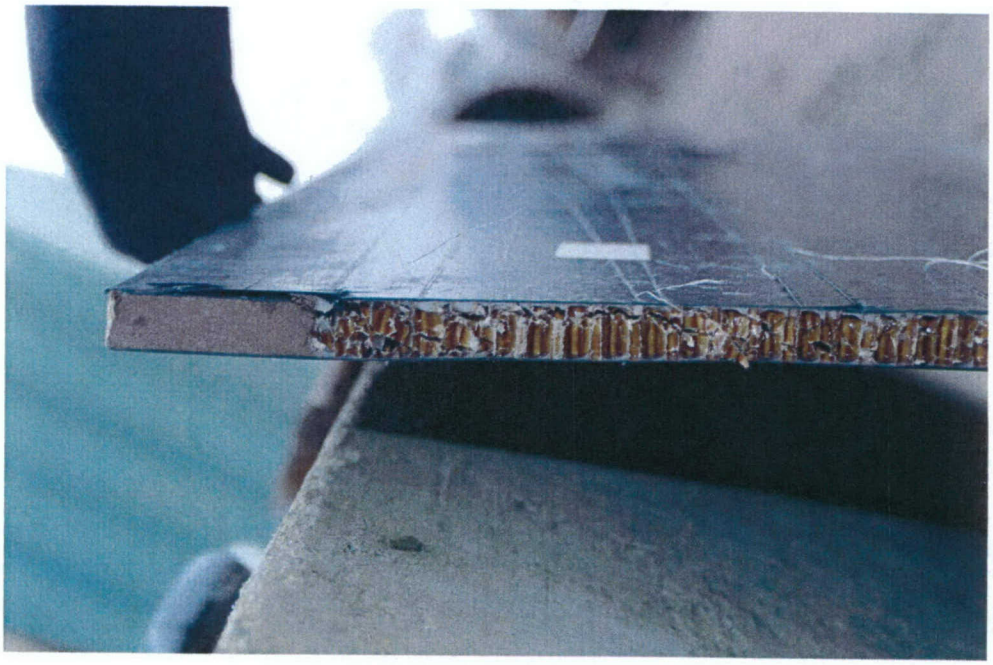

Figure C.8 In-plane cracks in the honeycomb, probably due to shear stresses.

D Material Characterization Tests

Rotterdamseweg 145
2628 AL Delft
The Netherlands
Phone: +31 15 251 34 30
Fax: +31 15 251 34 39
Website: www.ale.nl
E-mail: info@ale.nl
KvK nr.: 27169359
Bank nr.: ING 67 34 58 121

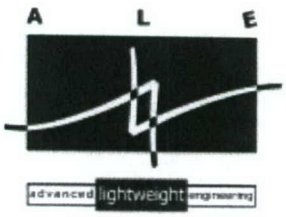

Material Characterization Tests

Report

for

TNO Prins Maurits Laboratory

Report: 04017-1-kve/ovj
Reference: 04.504
Author: Ir. K. Vervenne
Date: 17 December 2004

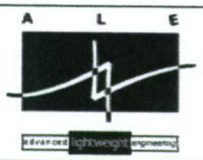

Advanced Lightweight Engineering BV
Rotterdamseweg 145
2628 AL Delft
☎ +31 15 251 3430
✉ +31 15 251 3439
info@ale.nl
www.ale.nl

Project number	04017
Principal	TNO Prins Maurits Laboratory
Author	Ir. K. Vervenne
Date	17 December 2004
Report number	04017-1-kve/ovj
Number of pages	17
Summary	TNO PML has asked ALE to determine tensile, in-plane shear and out-of-plane shear properties according to ASTM standards, as input data for a numerical ballistic model. The plates consist of plain weave AS4 carbon fiber in 3501 epoxy and were already tested ballistically. In addition the fiber volume fraction is estimated and one plate is C-scanned. The results of the mechanical tests derived from 3 samples per test were:

	Mean value	**Standard deviation**
F_x	431.4 MPa	22.4 MPa
F_{xy}	247.2 MPa	14.0 MPa
F_{xz}	33.8 MPa	4.0 Mpa
F_{zx}	28.2 MPa	1.4 MPa
E_x	44.9 GPa	2.0 Gpa
G_{xy}	17.6 GPa	0.7 Gpa
G_{xz}	3.6 GPa	0.1 Gpa
G_{zx}	3.3 GPa	0.6 Gpa
v_{xy}	0.31	0.02

The fiber volume fraction could not be measured accurately. However the fiber volume fraction is between 56% and 61%. The C-scan indicated clearly the damaged areas of plate D14.
It is recommended to initiate a dedicated test program to establish proper input data for the numerical model.

Keywords	Tensile test ASTM D3039, In-plane shear test ASTM D3518, Out-of-plane shear test ASTM D5379, Ignition loss, C-scan test, AS4 carbon fiber, ballistics	
Author	**Checked**	**Authorized**
Ir. K. Vervenne	Ir. P. Verspui	Dr. ir. H. de Boer
Issue	**Issue date**	**First issue**
1	17 December 2004	17 December 2004

Contents

2.2 Test setup and test procedure

All test were executed at RT. A 25-tons static test bench was used. The test procedure was as follows:

1. The strain gage wires were solded to the connecting wires
2. The sample was clamped in the upper clamp
3. The strain gages were zeroed
4. The force was zeroed
5. The sample was clamped in the lower clamp, this leads to a small clamping force in the specimen.
6. The crosshead was automatically moved to set the force to zero again.
7. The test was started and the data was recorded automatically
8. The sample failed
9. After failure the sample was removed from the bench
10. The bench was cleaned and ready for a new test

A picture of the test set-up for the tensile test is shown in figure 3.

Figure 3: Tensile test set-up

2.3 Tensile test results

All data can be found on the CD-ROM delivered with this report. This CD-ROM also contains pictures of the specimen after the test. In this paragraph only the stress-strain curves and the calculated results are given. All calculations were done according to ASTM D3039.

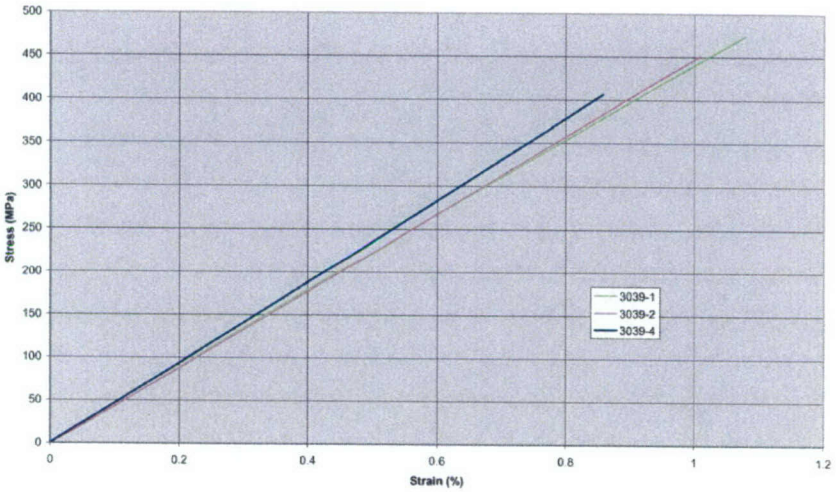

Figure 4: Stress-strain curves of the tensile test

	Ultimate stress	Ultimate strain	Modulus[1)]	ν_{xy}[1)]	Failure Mode[2)]
	MPa	%	GPa		
3039-1	435.425	1.079	43.037	0.291	LGM
3039-2	451.576	1.009	44.640	0.314	LGU
3039-4	407.280	0.858	47.023	0.329	LGU
Mean value	**431.427**	**0.982**	**44.900**	**0.311**	
SD	22.417	0.113	2.006	0.019	

[1)] The modulus and Poisson's ratio are determined between 0.1% and 0.3% strain

[2)] See the ASTM D3039 Standard for a description of these acronyms

Table 4: Results of the tensile test according to ASTM D3039

2.4 In-plane shear test results

All data can be found on the CD-ROM delivered with this report. This CD-ROM also contains pictures of the specimen after the test. In this paragraph only the stress-strain curves and the calculated results are given. All calculations were done according to ASTM D3518.

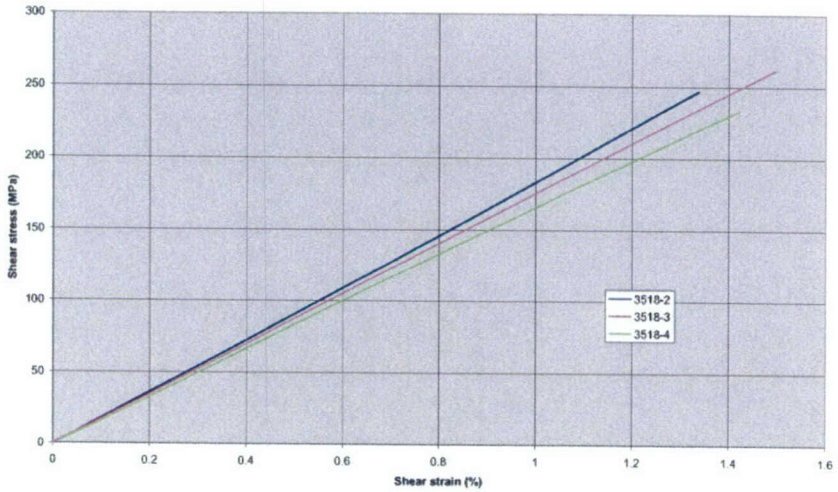

Figure 5: Stress-strain curves of the in-plane shear test

	Ultimate stress	Ultimate strain	Modulus[1)]	Failure Mode[2)]
	MPa	%	GPa	
3518-2	246.744	1.338	18.250	LGT
3518-3	261.587	1.497	17.668	LGU
3518-4	233.401	1.424	16.912	LGB
Mean value	**247.244**	**1.419**	**17.610**	
SD	14.099	0.080	0.671	

[1)] The modulus is determined between 0.2% and 0.6% strain

[2)] See the ASTM D3039 Standard for a description of these acronyms

Table 5:Results of the in-plane shear test according to ASTM D3518

3 Out-of-plane shear tests

First the characteristics of the samples are described, then the test-setup and test procedure is described, and finally the results are given. For a complete description of the test see the ASTM D5379 standard.

3.1 Specimen

The geometry of the specimen to determine the zx-shear properties is the same as the geometry of the specimen to determine the xz-shear properties and is described in figure 6:

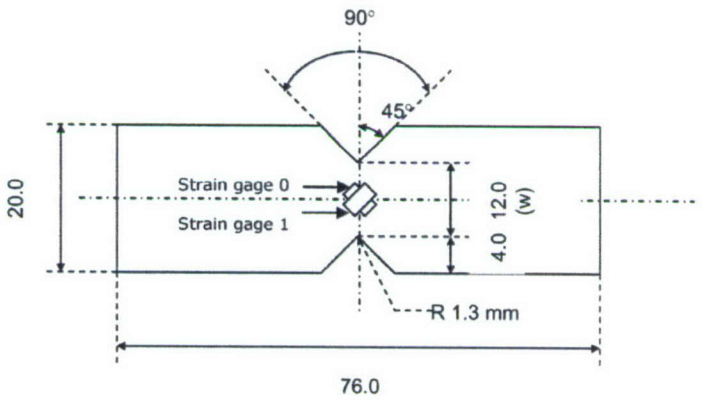

All in mm

Figure 6: Lay-out V-notch specimen (not to scale)

The specimen to determine the xz-shear properties can be made out of one piece, whereas the specimen of to determine the zx-shear properties, must be composed of three parts. This is shown in figure 7.
From TNO PML 4 xz-specimen and 12 zx-specimen were received with dimensions as indicated in figure 7. All these specimen were cut out of a plate by means of water jet cutting.
The zx-specimen were bonded in a mould to assure proper alignment, with epoxy adhesive mixed with micro-glass spheres and cured for 2 hours at 65°C.

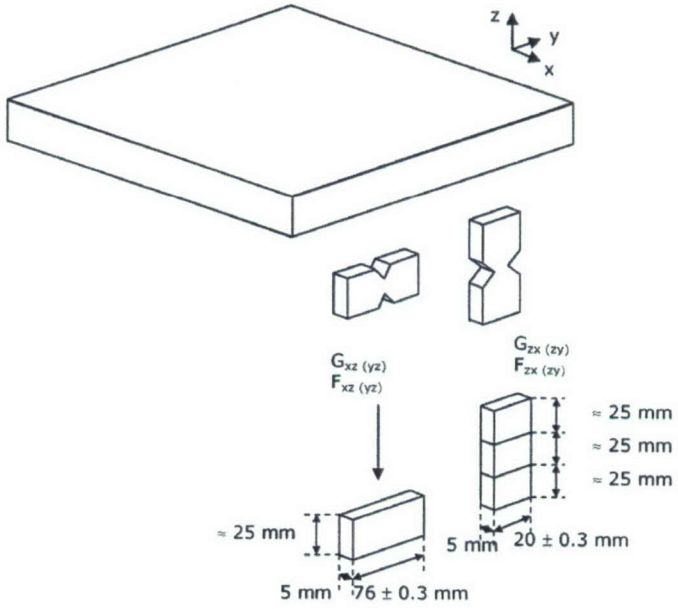

Figure 7: Out-of-plane shear specimen (not to scale)

All specimen were milled to the dimensions as indicated in figure 6. After that, all relevant dimensions were measured.

Sample ID	Cut from plate	Width[1)] (mm)	Thickness (mm)
XZ-1	G18	4.77	11.90
XZ-2	G18	5.41	11.92
XZ-3	G18	5.45	12.01
XZ-4	G18	Not tested	

[1)] w in figure 6

Table 6: Out-of-plane shear XZ sample dimensions

Sample ID	Cut from plate	Width[1)] (mm)	Thickness (mm)
ZX-1	G18	4.77	11.90
ZX-2	G18	Not tested	
ZX-3	G18	5.45	12.01
ZX-4	G18	5.28	12.00

[1)] w in figure 6

Table 7: Out-of-plane shear ZX sample dimensions

Strain gages were applied at the locations shown in figure 6. Type Kyowa KFG-2-120-D16-23 were used.

3.2 Test set-up and test procedure

All test were executed at RT. A 25-tons static test bench was used. The test procedure was as follows:

1. The sample was properly inserted in the V-notch test fixture
2. The strain gage wires were solded to the connecting wires

	Ultimate stress	Ultimate strain	Modulus[1)]
	MPa	%	GPa
xz-1	38.356	1.049	3.700
xz-2	30.528	0.875	3.479
xz-3	32.658	0.924	3.527
Mean value	**33.847**	**0.949**	**3.569**
SD	4.047	0.090	0.117

[1)] The modulus is determined between 0.25% and 0.6% strain

Table 8: Results of the out-of-plane xz-shear test according to ASTM D5379

The ultimate values are much lower than would be expected from the stress strain curves. However, according to ASTM5379, the first drop in force must be considered the ultimate value. This because after that point, the fibers are lining up with the load, and (as it clearly shows from the stress-strain curves) can still take a considerable load. This is however not a shear load anymore. The next picture shows a severely deformed specimen. The deformed and rearranged fibers can be seen clearly.

Figure 10: Specimen xz-3 at the end of the test

3.4 Out-of-plane zx-shear results

All data can be found on the CD-ROM delivered with this report. This CD-ROM also contains pictures of the specimen after the test. In this paragraph only the stress-strain curves and the calculated results are given. All calculations were done according to ASTM D5379.

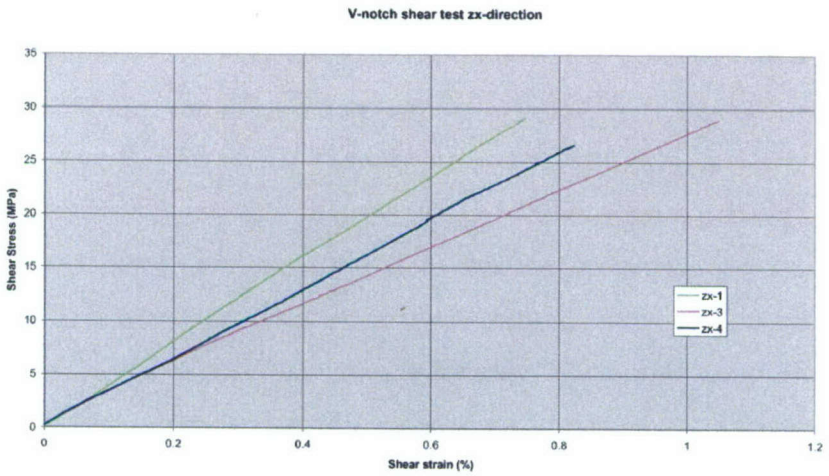

Figure 11: Stress-strain curves of the out-of-plane zx-shear test

	Ultimate stress	Ultimate strain	Modulus[1)]
	MPa	%	GPa
zx-1	29.092	0.747	3.839
zx-3	28.975	1.051	2.639
zx-4	26.557	0.823	3.333
Mean value	**28.208**	**0.874**	**3.270**
SD	1.431	0.158	0.603

[1)] The modulus is determined between 0.25% and 0.6% strain

Table 9:Results of the out-of-plane zx-shear test according to ASTM D5379

4 Ignition loss test

4.1 Fiber volume fraction

From the tested specimen small parts are cut with a saw. These parts are cleaned. Ceramic sample holders are cleaned and placed in an oven for 30 minutes at 565°C. After cooling the empty sample holders are weighed to the nearest 0.0001 g. The samples are placed in the sample holders and again weighed to the nearest 0.0001 g. Then the samples are placed in an oven at 565°C. At set time intervals the sample holders with samples are weighed. After about 10-15 minutes all epoxy resin is burned of. However, also the carbon fiber is affected and loses weight. Therefore the weighing is continued until the weight loss of the carbon fiber in time can be measured (assuming a linear decrease of weight in time). In this way the weight loss of the carbon fiber can be compensated.
Unfortunately this did not work for the V-notch specimen which were cut from a thick plate. Due to the combustion of the epoxy, the samples swelled, and not being hold together anymore by the epoxy resin, the carbon fibers flew out of the sample holders, thus making a correct measurement impossible. For the thinner tensile and in-plane specimen this effect was much less pronounced, and all the carbon fiber remained in the sample holders. However, a correct measurement was not possible, since the weight decrease of the carbon fiber was not linear. But assuming that all epoxy burnt of during the first 10-15 minutes and with the assumed density of AS4 fiber of 1790 kg/m3 and of the epoxy of 1200 kg/m3, a rough estimate still can be made:

Sample ID	Ignition loss after 12 minutes	Fiber volume fraction
	(%)	(%)
3039-1	32.0	59
3039-2	32.7	58
3039-4	34.4	56
3518-2	34.4	56
3518-3	34.5	56
3518-4	30.0	61

Table 10: Ignition loss and estimated fiber volume fraction

4.2 Laminate lay-up

When the epoxy is gone, the layers are no longer bonded together and the fiber orientations can be determined. The laminate lay-up turned out to be as follows:

Layer #	Orientation (°)
1	0/90
2	±45
3	0/90
4	±45
5	0/90
6	±45
7	±45
8	0/90
9	±45
10	0/90
11	±45
12	0/90

Table 11: Laminate lay-up for the tensile and in-plane shear test specimen

5 C-scan results

Plate D14 was scanned with a resolution of 1 mm in both x- and y-direction. With a threshold of 20 dB, the damaged and/or delaminated areas have been determined. The results can be found in figure 12. The black areas indicate damage. The white spots indicate holes. The area of the holes is not included in the damaged area.
On the CD-ROM the raw data file is included. This file can be used later for further evaluation.

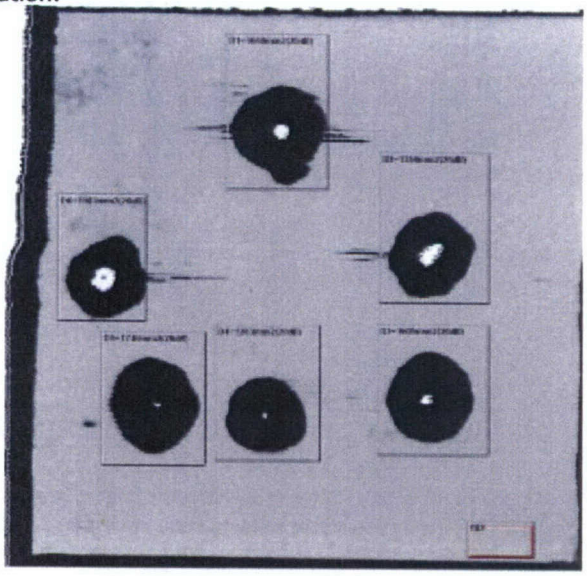

Figure 12: C-scan results

6 Summary and recommendations

The following values have been derived from the test:

	Mean value	Standard deviation
F_x	431.4 MPa	22.4 MPa
F_{xy}	247.2 MPa	14.0 MPa
F_{xz}	33.8 MPa	4.0 Mpa
F_{zx}	28.2 MPa	1.4 MPa
E_x	44.9 GPa	2.0 Gpa
G_{xy}	17.6 GPa	0.7 Gpa
G_{xz}	3.6 GPa	0.1 Gpa
G_{zx}	3.3 GPa	0.6 Gpa
ν_{xy}	0.31	0.02

Table 12: Summary of the test results

One must bear in mind that these values have derived from different plates, with it's own variations in exact fiber orientation, variations in resin properties due to different cure cycles and differences in fiber volume fraction. Therefore, selecting the results of one representative sample as input for the numerical model may lead to better results.

Furthermore it is recommended to implement a special test program in which dedicated specimen (with all manufacturing parameters known) are tested to obtain all necessary input parameters of the numerical model and for validation of the results from the numerical model.

REPORT DOCUMENTATION PAGE
(MOD-NL)

1. DEFENCE REPORT NO (MOD-NL)	2. RECIPIENT'S ACCESSION NO	3. PERFORMING ORGANIZATION REPORT NO
TD2005-0013		DV2 2005-A13
4. PROJECT/TASK/WORK UNIT NO	**5. CONTRACT NO**	**6. REPORT DATE**
014.14186	B02Klu500	March 2005
7. NUMBER OF PAGES	**8. NUMBER OF REFERENCES**	**9. TYPE OF REPORT AND DATES COVERED**
70 (incl 4 appendices, excl RDP & distribution list)	14	Final

10. TITLE AND SUBTITLE

Analysing blast and fragment penetration effects on composite helicopter structures

11. AUTHOR(S)

C. van 't Hof, K. Herlaar, J.M. Luyten, M.J. van der Jagt

12. PERFORMING ORGANIZATION NAME(S) AND ADDRESS(ES)

TNO Defence, Security and Safety, P.O. Box 45, 2280 AA Rijswijk, The Netherlands
Lange Kleiweg 137, Rijswijk, The Netherlands

13. SPONSORING AGENCY NAME(S) AND ADDRESS(ES)

DMKLu, P.O. Box 20703 2500 ES The Hague, The Netherlands

14. SUPPLEMENTARY NOTES

The classification designation Ongerubriceerd is equivalent to Unclassified.

15. ABSTRACT (MAXIMUM 200 WORDS (1044 BYTE))

Sandwich structures become increasingly important as structural parts in helicopters. This does not only have effect on the way of construction but also on the vulnerability of the helicopter. The last decades the threat of helicopters has increased in military circumstances. Consequently the helicopters will be exposed to weapon effects like high blast loads and fragment impact more frequently. Moreover the blast load becomes more important because the threat comes closer to the target.

At TNO different blast and fragment response models are available for metal structures. However little is known about the blast and fragment performance of sandwich panels. To be able to determine the damage of these structures due to blast loads and fragment impact it will be necessary to extend the present vulnerability methods for composite structures.

A combination of numerical simulations and experiments were performed for both blast loading and fragment impact on composite structures. The numerical results show good agreement with the experiments but must be improved for some applications. The numerical tools make it possible in future to simulate vulnerability of composite structures without the need of large and expensive experiments.

16. DESCRIPTORS	IDENTIFIERS
Composite material	Helicopter
Sandwich	Panel
Blast load	Vulnerability
Fragment impact	Finite element modelling

17a. SECURITY CLASSIFICATION (OF REPORT)	17b. SECURITY CLASSIFICATION (OF PAGE)	17c. SECURITY CLASSIFICATION (OF ABSTRACT)
Ongerubriceerd	Ongerubriceerd	Ongerubriceerd

18. DISTRIBUTION AVAILABILITY STATEMENT	17d. SECURITY CLASSIFICATION (OF TITLES
Unlimited Distribution	Ongerubriceerd

Onderstaande instanties/personen ontvangen een volledig exemplaar van het rapport.

1	SC-WOO
2	HWO-KLu
3	Programmabegeleider Defensie, Lt-kol. B.H. Hoitink, KLu
4	Projectbegeleider Defensie Lt-kol. Ing. J. Helderman, KLu
5/7	Bibliotheek KMA
8	TNO Defensie en Veiligheid, vestiging Rijswijk, daarna reserve Manager Business Unit Bescherming, Munitie en Wapens (operaties), ir. P.J.M. Elands
9	TNO Defensie en Veiligheid, vestiging Rijswijk, Manager Business Unit Bescherming, Munitie en Wapens (kennis), Mw. ir. E.N. van Son-de Waard
10	TNO Defensie en Veiligheid, vestiging Rijswijk, Manager Business Unit Bescherming, Munitie en Wapens (markt) dr. ir. L.H.J. Absil
11	Programmaleider TNO Defensie en Veiligheid, R. le Fevre
12/13	TNO Defensie en Veiligheid, vestiging Rijswijk, Informatie- en Documentatiedienst
14/20	TNO Defensie en Veiligheid, vestiging Rijswijk, Business Unit Bescherming, Munitie en Wapens, ir. A. Schilt, ir. J.M. Luyten, ir. K. Herlaar, ir.ing. C. van 't Hof, ir. M.J. van der Jagt, ing. A.G. van Erkel en ir. J.J.M. Paulissen
21	TNO Defensie en Veiligheid, vestiging Rijswijk, Marketing en Communicatie, digitale versie via Archief

Distributionlist

Onderstaande instanties/personen ontvangen het managementuittreksel en de distributielijst van het rapport.

4 ex.	SC-WOO
8 ex.	HWO-KL
4 ex.	HWO-KLu
5 ex.	HWO-KM
4 ex.	HWO-CO
1 ex.	TNO Defensie en Veiligheid, Algemeen Directeur, ir. P.A.O.G. Korting
3 ex.	TNO Defensie en Veiligheid, Directie Directeur Operaties, ir. C. Eberwijn Directeur Kennis, prof. dr. P. Werkhoven Directeur Markt, G.D. Klein Baltink
1 ex.	TNO Defensie en Veiligheid, dr. D.W. Hoffmans
1 ex.	TNO Defensie en Veiligheid, accountdirector KLu
1 ex.	TNO Defensie en Veiligheid, vestiging Den Haag, Manager Business Unit Waarnemingssystemen (operaties), dr. M.W. Leeuw
1 ex	TNO Defensie en Veiligheid, vestiging Den Haag, Manager Business Unit Beleidsstudies Operationele Analyse & Informatie Voorziening (operaties), drs. T. De Groot
1 ex	TNO Defensie en Veiligheid, vestiging Rijswijk, Manager Business Unit BC Bescherming (operaties), ir. R.J.A. Kersten
1 ex	TNO Defensie en Veiligheid, vestiging Soesterberg, Manager Business Unit Gedrag, Training & Prestatie (operaties), drs. H.J. Vink
1 ex.	TNO Defensie en Veiligheid, vestiging Soesterberg , Communicatiemanager TNO Defensie en Veiligheid, P.M. van Bergem-Jansen
1 ex.	Lid Instituuts Advies Raad DenV BGen. prof. J.M.J. Bosch
1 ex.	Lid Instituuts Advies Raad DenV Cmdr. b.d. drs. G.M.W. Acda
1 ex.	Lid Instituuts Advies Raad DenV prof. dr. ir. M.P.C.Weijnen